

# Turbulent mass transfer through a flat shear-free surface

By JACQUES MAGNAUDET<sup>1</sup> AND ISABELLE CALMET<sup>2</sup>

<sup>1</sup>Institut de Mécanique des Fluides de Toulouse, UMR 5502, 2 allée Camille Soula,  
31400 Toulouse, France

<sup>2</sup>Ecole Centrale de Nantes, UMR 6598, 1 rue de la Noe, 44321 Nantes cedex 3, France

(Received 15 April 2005 and in revised form 29 September 2005)

Mass transfer through the flat shear-free surface of a turbulent open-channel flow is investigated over a wide range of Schmidt number ( $1 \leq Sc \leq 200$ ) by means of large-eddy simulations using a dynamic subgrid-scale model. In contrast with situations previously analysed using direct numerical simulation, the turbulent Reynolds number  $Re$  is high enough for the near-surface turbulence to be fairly close to isotropy and almost independent of the structure of the flow in the bottom region (the statistics of the velocity field are identical to those described by I. Calmet & J. Magnaudet *J. Fluid Mech.* vol. 474, 2003, p. 355). The main statistical features of the concentration field are analysed in connection with the structure of the turbulent motion below the free surface, characterized by a velocity macroscale  $u$  and an integral length scale  $L$ . All near-surface statistical profiles are found to be  $Sc$ -independent when plotted *vs.* the dimensionless coordinate  $Sc^{1/2}yu/\nu$  ( $y$  is the distance to the surface and  $\nu$  is the kinematic viscosity). Mean concentration profiles are observed to be linear throughout an inner diffusive sublayer whose thickness is about one Batchelor microscale, i.e.  $LSc^{-1/2}Re^{-3/4}$ . In contrast, the concentration fluctuations are found to reach their maximum near the edge of the outer diffusive layer which scales as  $LSc^{-1/2}Re^{-1/2}$ . Instantaneous views of the near-surface isovalues of the concentration and vertical velocity are used to reveal the influence of the Schmidt number. In particular, it is observed that at high Schmidt number, the tiny concentration fluctuations that subsist in the diffusive sublayer just mirror the divergence of the two-component surface velocity field. Co-spectra of concentration and vertical velocity fluctuations indicate that the main contribution to the turbulent mass flux is provided by eddies whose horizontal size is close to  $L$ , which strongly supports the view that the mass transfer is governed by large-scale structures. The dimensionless mass transfer rate is observed to be proportional to  $Sc^{-1/2}$  over the whole range of Schmidt number. Based on a frequency analysis of the concentration equation and on the  $Sc^{-1/2}Re^{-3/4}$  scaling of the diffusive sublayer, it is shown that the mass transfer rate at a given  $Sc$  is proportional to  $\langle \beta^2 \rangle^{1/4}$ ,  $\langle \beta^2 \rangle$  being the variance of the divergence of the surface velocity field. This yields dimensionless mass transfer rates of the form  $\alpha Sc^{-1/2}Re^{-1/4}$ , where the value of  $\alpha$  is shown to result from both the kinematic blocking of the vertical velocity and the viscous damping of the horizontal vorticity components induced by the free surface.

---

## 1. Introduction

The transfer of weakly soluble gases through gas–liquid interfaces is of paramount importance in geophysical and industrial processes. In particular, it is central in

pollution and climate change problems since it governs the balance of carbon dioxide ( $\text{CO}_2$ ) and other greenhouse gases between the atmosphere and the oceans or the lakes. Similarly, falling films and bubbly flows are widely used as mass exchangers in chemical reactors. The difficulty in the parameterization of the rate at which weakly soluble gases penetrate into the liquid phase in such systems stems from the fact that the resistance to the transfer is essentially concentrated within a very thin sublayer of liquid where turbulence is reduced (because of the surface boundary condition on the vertical velocity) and molecular diffusion becomes dominant. The thinness of this diffusive layer (typically  $10\text{--}10^2\ \mu\text{m}$  for  $\text{CO}_2$ ) is a very severe obstacle to local measurements of the concentration and velocity required to elucidate many aspects of the transfer process. Therefore, for decades, only global measurements were performed in several laboratory or field flow configurations. The corresponding data were then used to develop models relating the mass transfer rate to the physical properties of the liquid and dissolved gas and to some of the macroscopic characteristics of the flow. This gave rise to two main families of mass transfer models.

The first of these is based on the concept of eddy diffusivity (Levich 1962; Davies 1972). Paralleling Prandtl's ideas of eddy viscosity and mixing length, eddy diffusivity models consider globally the effect of all turbulent scales and express the turbulent mass flux at a certain distance from the surface as a function of the local momentum flux. Integration through the concentration boundary layer then yields directly the mass flux at the surface. The main conceptual limitation of these models is that they make use of some sort of Reynolds analogy. Moreover, even in situations where this analogy holds, as in wall-bounded shear flows, the determination of the model coefficients is uncertain, especially in the transition region where the transfer is controlled both by molecular diffusion and turbulence. The situation is worse at a free surface, since the Reynolds analogy does not hold because the scalar flux and the momentum flux evolve differently with the distance to the surface.

The second family of models is based on the concept of renewal eddies that 'refresh' the fluid elements at the gas-liquid interface. These models state that the average velocity  $K_L$  at which the gas dissolves into the liquid is controlled by its molecular diffusivity  $D$  and by a so-called renewal time scale  $\tau$ . From dimensional evidence, Highbie (1935) and Danckwerts (1951) then obtained  $K_L = (D/\tau)^{1/2}$ . The key problem is then the prediction of the time scale  $\tau$ . Two different viewpoints, based on separate experimental data sets, emerged in the late 1960s. Fortescue & Pearson (1967) studied the absorption of  $\text{CO}_2$  in an open-channel flow in which turbulence was enhanced by a vertical grid placed near the entrance section. Their results supported the view that mass transfer is controlled by large-scale eddies, i.e.  $\tau \propto \Lambda/u_0$ , where  $\Lambda$  is some measure of the turbulence macroscale and  $u_0$  characterizes the magnitude of large-scale velocity fluctuations. In dimensionless form, this yields  $K_L/u_0 \propto Sc^{-1/2} Re_A^{-1/2}$ , where  $Re_A = \Lambda u_0/\nu$  is the turbulent Reynolds number and  $Sc = \nu/D$  is the Schmidt number,  $\nu$  denoting the kinematic viscosity of the liquid. On the other hand, Banerjee, Rhodes & Scott (1968) and Lamont & Scott (1970) performed  $\text{CO}_2$ -absorption experiments in a falling film and in a bubbly pipe flow, respectively. They found that their data correlated properly using the Kolmogorov time scale  $(\nu/\varepsilon)^{1/2}$  as the characteristic time scale  $\tau$  ( $\varepsilon$  being the dissipation rate per mass unit), which suggests that the absorption process is controlled by small-scale eddies. Since the dissipation rate may be expressed in terms of large-scale characteristics through Taylor's relationship  $\varepsilon \propto u_0^3/\Lambda$  (Batchelor 1953, p. 103), this yields in dimensionless form  $K_L/u_0 \propto Sc^{-1/2} Re_A^{-1/4}$ . Hence the two different scalings yield conflicting exponents of the turbulent Reynolds number in the expression of

$K_L/u_0$ . This problem launched a long controversy as to which range of scales is the most efficient in the high-Schmidt-number mass transfer mechanism. Data available up to 1975 were critically re-examined by Theofanous, Houze & Brumfield (1976) who suggested that there is a smooth transition between a low- $Re_A$  regime in which the large-scale eddies control the transfer and a high- $Re_A$  regime where small-scale eddies dominate, the transition between the two regimes taking place for  $Re_A \approx 500$ .

The next conceptual step was achieved with the recognition of the central role played by the surface divergence of interfacial motions. In a comprehensive study, McCready, Vassiliadou & Hanratty (1986) solved numerically a simplified two-dimensional form of the concentration equation in which the normal velocity fluctuation was expanded in the form  $\beta(t)y$  very close to the surface (assumed to lie in the plane  $y=0$ ), the strain rate  $\beta(t)$  being taken from the time series of a near-wall experimental signal. Their results indicated that  $K_L/u_0$  depends linearly on  $\langle\beta^2\rangle^{1/4}$ , which is in line with the surface renewal concept, provided the characteristic time is selected to be  $\tau \propto \langle\beta^2\rangle^{-1/2}$ . Obviously, the renewal model based on the latter scaling is more general than the 'large-scale' and 'small-scale' models discussed above, as  $\langle\beta^2\rangle$  results from an integration over the whole spectrum of near-surface motions. In particular, this model suggests that all frequencies of the near-surface flow contribute to the transfer efficiency, in contrast with the near-wall situation where a similar approach proved the mass transfer to be controlled by low-frequency events (Campbell & Hanratty 1983). Based on the conclusions of McCready *et al.* (1986) and on the idealized inviscid description of the distortion of the bulk turbulence by a flat surface (Hunt & Graham 1978), several authors then attempted to obtain an explicit expression of  $\langle\beta^2\rangle$  as a function of the characteristics of the turbulence in the bulk (Brumley & Jirka 1988; Banerjee 1990). Such models were recently found to perform well when compared with mass transfer data obtained in open channels as well as in grid-stirred tanks (Banerjee, Lakehal & Fulgosi 2004).

In parallel with this evolution of conceptual models, investigation techniques improved, especially during the last two decades. More detailed measurements of the near-surface concentration field were made possible by laser-induced fluorescence (LIF) techniques (Asher & Pankow 1986; Woodrow & Duke 2001; Herlina & Jirka 2004), as well as by the development of microprobes capable of following concentration fluctuations (Chu & Jirka 1992). However, these techniques still have difficulties in resolving the uppermost layers of the flow. Moreover, the attempts made at a simultaneous determination of the concentration and velocity fields (required to obtain directly the profile of the turbulent mass flux) have been inconclusive up to now. In contrast, particle image velocimetry (PIV) techniques now allow the near-surface eddies and the surface velocity field to be adequately resolved (see e.g. Kumar, Gupta & Banerjee 1998; McKenna & McGillis 2004).

During the same period, several groups carried out direct numerical simulations (DNS) of open-channel flow (Handler *et al.* 1993; Komori *et al.* 1993; Borue, Orszag & Staroselsky 1995; Pan & Banerjee 1995). In most of these studies, emphasis was put on the connection between the ejection of hairpin vortices from the bottom boundary layer and the large-scale structures in the near-surface region. The most recent DNS in the same flow configuration included passive heat/mass transfer through the free surface at Prandtl/Schmidt number ranging from 1 to 5 (Lu & Hetsroni 1995; Handler *et al.* 1999; Nagaosa 1999; Yamamoto, Kunugi & Serizawa 2001). These studies proved very useful in establishing detailed statistics of the dynamic and scalar fields which are still far beyond the capabilities of laboratory experiments. Moreover, they revealed a number of important features concerning the connection between

the vortices ejected from the bottom region and the topology of the near-surface concentration field.

The main limitation of these DNS studies stems of course from their low Reynolds number. The corresponding turbulent Reynolds number  $Re^*$  based on the friction velocity at the bottom wall and flow depth ranges typically from 150 to 200, which forces the free surface to lie within the logarithmic layer of the mean velocity profile. Therefore the turbulence 'seen' by the free surface is strongly anisotropic and interacts directly with the vigorous dynamics of the bottom region. This makes the structure of the near-surface dynamical and scalar fields observed in these DNS quite specific to low-Reynolds-number wall-bounded shear flows and prevents some of the important conclusions of these studies from applying directly to flows of geophysical relevance. It is thus desirable to develop a detailed analysis of the instantaneous and statistical structure of the velocity and concentration fields in free-surface flows where turbulence is closer to isotropy and less dependent on the precise way it is generated, as has long been achieved experimentally by using grid-stirred tanks (Chu & Jirka 1992; McKenna & McGillis 2004). Moreover, increasing the turbulent Reynolds number compared to that of the aforementioned DNS is necessary to remove low-Reynolds-number effects and obtain predictions valid in high-Reynolds-number flows. This programme was partly applied by Calmet & Magnaudet (2003, hereinafter referred to as CM) who used large-eddy simulation (LES) to analyse the statistical structure of the near-surface region of a high-Reynolds-number open-channel flow in which  $Re^*$  was about  $1.3 \times 10^3$ . This high value of the Reynolds number allowed the existence of an upper region of the flow where turbulence was approximately isotropic and shear-free and resembled that produced in a grid-stirred tank, even though some well-identified quantitative differences exist and the two generating mechanisms are totally different (the near-surface turbulence is generated by the bursting process in an open-channel flow, by the interaction of vertical jet-like motions created by the grid oscillation in a grid-stirred tank). Among other things, this study allowed a detailed and successful comparison of numerical results with the theory elaborated by Hunt & Graham (1978) to describe the distortion of a homogeneous isotropic turbulence by a flat rigid surface; as similar conclusions were obtained experimentally by Brumley & Jirka (1987) in a grid-stirred tank, this reinforces the above view that the two types of flow exhibit near-surface regions with a similar turbulence structure.

The present paper reports on the next step of the same programme. That is, starting from the velocity field discussed in CM, we perform several LES runs to compute the evolution of the concentration field of gases of various diffusivities absorbed through the free surface of the flow. The Schmidt number is varied from 1 to 200, the latter value being approximately that of helium in water. In contrast, the Reynolds number is kept fixed, but we shall see that conclusions concerning its influence on several statistical quantities can be obtained, either by order-of-magnitude arguments or by comparison with available low-Reynolds-number DNS. The main questions we wish to address in this investigation are the following. What is the statistical structure of the mean and fluctuating near-surface concentration field? How does the thickness of the various concentration sublayers evolve with the Schmidt and Reynolds number? How are instantaneous near-surface concentration and velocity fluctuations connected with each other? What are the characteristic scales of the eddies involved in the transfer? How does the average mass transfer velocity at the surface depend on the Schmidt number and on the near-surface turbulence characteristics? In line with the state-of-the-art summarized above, we think high-Reynolds-number LES results provide new

insights on these questions and usefully complement the views offered by available experimental and numerical results.

An important point in the work reported below concerns the scaling of the results. In the DNS studies mentioned above, the results were always normalized using the velocity scale  $u^*$  and the length scale  $\nu/u^*$ . While these wall variables are relevant when analysing wall-bounded flows, they are not appropriate to describe shearless turbulence near a free surface and derive general scaling laws for this type of flow (see §3 of CM). Indeed, as turbulence is produced ‘far’ from the region of interest, a proper normalization must be independent of the precise nature of its source. Moreover, as soon as the concentration field is concerned, it is obvious that the relevant vertical length scales in the near-surface region depend on the gas diffusivity, i.e. on the Schmidt number. Particular attention is paid to these aspects in the following sections, the goal being to make the results as ‘flow’- and ‘gas’-independent as possible. The structure of the paper is as follows. Aspects of the numerical procedure specific to the present study are presented in §2. Section 3 deals with the scaling aspects mentioned above and analyses the first- and second-order one-point statistics of the concentration field near the free surface. Section 4 is devoted to the connection between the instantaneous concentration field and the near-surface turbulent motions. Section 5 focuses on the scaling of the average mass transfer rate and its connection with the dynamics of the near-surface flow. Summary and suggestions for future work are provided in §6.

## 2. Numerical procedure

The numerical code employed in this study, the filtering procedures and the dynamic closure strategy used for evaluating the subgrid-scale stresses and fluxes have been described in Calmet & Magnaudet (1997). Their application to the present flow configuration, as well as the grid characteristics required to simulate properly the corresponding large-scale velocity field have been detailed in CM. Here, we only summarize briefly those aspects that are most closely related to the computation of the large-scale concentration field.

Once filtered by the computational grid, the conservation equation for the concentration reads

$$\frac{\partial \bar{C}}{\partial t} + \frac{\partial}{\partial x_j} (\bar{C} \bar{V}_j) = \frac{\partial}{\partial x_j} \left[ D \frac{\partial \bar{C}}{\partial x_j} - q_j \right], \quad (1)$$

where  $\bar{V}_i$  is the  $i$ th component of the resolved velocity field,  $\bar{C}$  is the resolved concentration field and the  $q_i = \overline{C \bar{V}_i} - \bar{C} \bar{V}_i$  are the subgrid-scale fluxes to be modelled. Following Germano’s (1986) decomposition, the  $q_i$  are found to comprise a so-called Leonard contribution  $\overline{C \bar{V}_i} - \bar{C} \bar{V}_i$  which may be directly evaluated by re-filtering the resolved concentration and velocity fields and their product, and a contribution involving the unresolved velocity and/or concentration. The latter is modelled using a subgrid-scale diffusivity model in which the diffusivity is of the form  $D_T = C_C \bar{\Delta}^2 |\bar{S}|$  (Smagorinsky 1963),  $\bar{\Delta} = (\bar{\Delta}_1 \bar{\Delta}_2 \bar{\Delta}_3)^{1/3}$  being the local averaged grid scale ( $\bar{\Delta}_i$  is the grid size in the direction  $i$ ) and  $\bar{S} = (2\bar{S}_{ij} \bar{S}_{ij})^{1/2}$  being the local magnitude of the filtered strain rate ( $\bar{S}_{ij}$  is the filtered strain rate tensor). Thus, we finally write

$$q_i = -C_C \bar{\Delta}^2 |\bar{S}| \frac{\partial \bar{C}}{\partial x_i} + \overline{C \bar{V}_i} - \bar{C} \bar{V}_i. \quad (2)$$

Similarly to the procedure used for the subgrid-scale viscosity, the parameter  $C_c$  involved in (2) is dynamically computed at each time step by evaluating the difference between the  $q_i$  and the subgrid scalar fluxes corresponding to a test grid of size  $2\Delta$  and making use of Germano's (1992) identity. A local volume filtering of  $C_c$  is carried out to prevent the occurrence of negative values of the total diffusivity  $D + D_T$  to occur.

The geometry of the flow configuration and the boundary conditions are as follows. The flow is driven by a constant pressure gradient along the  $x$ -direction and periodic boundary conditions for the filtered velocity and concentration fields are assumed in this direction, as well as in the spanwise ( $z$ ) direction. In the vertical ( $y$ ) direction, the filtered velocity field obeys a no-slip condition at the bottom wall  $y = 2\delta$  ( $\delta$  being the channel half-height) and a shear-free condition at the free surface  $y = 0$ ; this is made possible by setting the average pressure gradient to the value  $-\langle\tau\rangle/2\delta$ ,  $\langle\tau\rangle$  denoting the averaged shear stress at the bottom wall. We assume that the renewal time of the diffused species at the free surface is smaller than the smallest time scale involved in the velocity field, which implies that the filtered concentration keeps a constant value, say  $\bar{C} = 1$ , at the surface. To drive the diffused species into the liquid and allow its concentration to reach a statistically stationary distribution,  $\bar{C}$  is assumed to keep a different constant value, say  $\bar{C} = 0$ , at the bottom wall. The concentration field is initialized with the pure diffusion profile  $\bar{C}(x, y, z, t = 0) = 1 - y/2\delta$ .

The underlying flow field is identical to that computed and discussed in CM, with a flow Reynolds number  $Re^* = 2u^* \delta/\nu$  based on the friction velocity  $u^* = (\langle\tau\rangle/\rho)^{1/2}$  ( $\rho$  being the fluid density) set to 1280. As shown in CM, when the flow has reached a statistically steady state, the resulting integral length scale  $L$  in the core is about  $0.4\delta$ . Thanks to the high value of  $Re^*$ , the large-scale turbulent field at  $y = L$ , i.e. below the near-surface region within which the surface distorts the turbulent field, is fairly close to isotropy with almost identical values of the vertical and spanwise r.m.s. velocities and a streamwise r.m.s. velocity 30% larger than the latter two. The corresponding velocity macroscale  $u$  (defined so that the averaged turbulent kinetic energy at  $y = L$  equals  $3u^2/2$ ) is about  $0.7u^*$ , yielding a turbulent Reynolds number  $Re = 2Lu/\nu$  about 360 (see § 5.1 of CM).

The computations are carried out in a parallelepipedic box of size  $2\pi\delta \times 3\pi\delta/4$  in the horizontal ( $x, z$ )-plane (see CM for the choice of this size). The spatial discretization in the ( $x, z$ )-plane is uniform and makes use of  $32 \times 64$  points. In the vertical direction, a non-uniform grid with either 68 or 82 points is used, depending on the value of the Schmidt number. The  $y$ -distribution of the grid points is designed so that at least three points lie within the diffusive sublayer located below the surface. For  $Sc = 1$ , this distribution is symmetric with respect to the midplane  $y = \delta$ , the smallest mesh spacing  $\Delta y$  near the two boundaries being such that  $\Delta y^+ = u\Delta y/\nu \approx 0.7$ . As we expect the thickness of the diffusive sublayer near the free surface to decrease strongly when the Schmidt number increases, the upper part of the grid is refined for higher Schmidt numbers. To keep the computation accurate up to  $Sc = 200$ , the minimum grid spacing is reduced to  $\Delta y^+ \approx 0.056$  on the finest grid. After the flow has reached a statistical equilibrium (characterized in particular by a linear vertical distribution of the averaged shear stress), time integration is pursued over five to ten turnover times to obtain converged first- and second-order statistics of the concentration field. These statistics are obtained by averaging in time as well as in the horizontal directions  $x$  and  $z$ . In the following, for any variable  $\Phi$  whose resolved value is  $\bar{\Phi}$ ,  $\langle\Phi\rangle$  denotes the corresponding average and  $\varphi''$  is the resolved fluctuation, i.e. we have  $\bar{\Phi} = \langle\bar{\Phi}\rangle + \varphi''$ , whereas if all scales were resolved we would access the total fluctuation  $\varphi'$  such that  $\Phi = \langle\Phi\rangle + \varphi'$ .

### 3. One-point statistics of the concentration field

#### 3.1. Scaling

As pointed out in §1, the Reynolds number of the present LES is typically five times larger than that of available low-Reynolds-number DNS of open-channel flow, which makes the turbulence near the free surface only weakly influenced by the detailed structure of the bottom region. Hence, the most relevant characteristics of the large-scale near-surface turbulent field are the velocity scale  $u$  and the integral length scale  $L$  defined above. Using these normalization scales, present results can be directly compared with those obtained in other almost equivalent configurations, such as grid-stirred tanks.

The normalization of concentration fluctuations deserves some more care. It is customary in the fluid mechanics literature to normalize the concentration difference  $1 - \langle \bar{C} \rangle$  and the resolved fluctuation  $c''$  by a reference surface concentration  $c$  defined through the relation  $cu = D|\partial\langle\bar{C}\rangle/\partial y|_{y=0}$ . The quantity  $c$  may be thought of as a measure of the surface mass flux in a given turbulent field. In the chemical engineering literature, it is generally preferred to use the concentration difference  $\Delta C = 1 - C_b$  where  $C_b$  is the mean concentration in the bulk. It will be shown below that both normalizations are useful when considering statistical quantities associated with very different Schmidt numbers. The magnitude of near-surface quantities involving the concentration fluctuation alone experiences little variation with the Schmidt number, whereas those involving the correlation between the concentration and velocity fluctuations strongly decrease when the Schmidt number increases. As  $\Delta C$  follows the former trend whereas  $c$  follows the latter, it is suitable when dealing with a wide range of Schmidt number to normalize quantities such as the r.m.s. of  $c''$  by  $\Delta C$ , while normalizing the concentration fluctuation involved in quantities such as the turbulent flux by  $c$ . In what follows,  $\Delta C$  will be determined by defining the bulk concentration  $C_b$  as the mean concentration at a distance  $y = L$  from the free surface, i.e.  $\Delta C = 1 - \langle \bar{C} \rangle(y = L)$ . With this definition,  $\Delta C$  ranges from 0.456 for  $Sc = 1$  to 0.494 for  $Sc = 200$ . Note that  $c$  and  $\Delta C$  are both characteristic of the mass transfer at the free surface, and do not depend on the transfer at the bottom wall.

To analyse the dynamics of the surface boundary layer, the relevant inner length scale is obviously  $y^+ = yu/\nu$ . It is also customary to use this viscous length scale in the discussion of the characteristics of the concentration boundary layer. Nevertheless it can be shown that a more relevant length scale incorporating directly the main effect of the Schmidt number can be built. For this purpose, let us start by normalizing (1) using the scales  $u$  and  $c$ . Averaging and integrating once with respect to  $y$  then yields

$$\frac{1}{Sc} \frac{\partial \langle \bar{C} \rangle^+}{\partial y^+} + \langle c'' v'' \rangle^+ + \langle q_2 \rangle^+ = 1, \quad (3)$$

where  $\langle \bar{C} \rangle^+ = (1 - \langle \bar{C} \rangle)/c$ ,  $\langle c'' v'' \rangle^+$  and  $\langle q_2 \rangle^+$  being the dimensionless resolved and subgrid vertical mass fluxes, respectively. When  $y^+ \rightarrow 0$ , the last two terms on the left-hand side of (3) vanish, and the local mass flux is dominated by molecular diffusion. This results in a diffusive sublayer where  $\langle \bar{C} \rangle^+$  follows the linear evolution  $\langle \bar{C} \rangle^+ = Sc y^+$ . Within this sublayer, the dimensionless fluctuation  $c''^+ = c''/c$  may be expanded as  $c''^+ = ay^+ + O(y^{+3})$ , the  $O(y^{+2})$  contribution being zero because  $\partial^2 c''/\partial y^2$  is zero at the surface, as may be seen by expanding (1) near  $y = 0$ . Similarly, within the viscous sublayer in which the vertical gradients of the horizontal velocity fluctuations fall to zero to satisfy the shear-free condition, the vertical velocity fluctuation evolves as  $v''^+ = by^+ + O(y^{+3})$  (here the  $O(y^{+2})$  contribution vanishes owing to continuity).

From the above expansions, we conclude that provided  $Sc \geq 1$ , the averaged resolved turbulent flux evolves as  $\langle c''v'' \rangle^+ = \langle ab \rangle y^{+2} + O(y^{+4})$  throughout the diffusive sublayer,  $\langle ab \rangle$  being a function of both  $Re$  and  $Sc$  (the condition  $Sc \geq 1$  is required to ensure that  $v''$  evolves linearly throughout the diffusive sublayer). However, within the diffusive sublayer, effects of the molecular diffusivity dominate and there is no reason for  $c''^+$  to depend on viscosity (at least at leading order), as  $c''^+$  is a relative fluctuation normalized by the surface value  $c$  which already takes into account the main effects of the viscosity through its dependence with respect to  $Re$  and  $Sc$ . Hence, for  $ay^+$  to be independent of the viscosity,  $a$  must be a linear function of  $Sc$ , and so is  $\langle ab \rangle$ . Then we may determine the dimensionless distance  $\delta_c^+$  to the surface at which the molecular and turbulent contributions to the concentration flux reach a similar magnitude, i.e. the location where the dimensionless turbulent diffusivity  $\langle ab \rangle Sc y^{+2} / (\partial \langle \bar{C} \rangle^+ / \partial y^+)$  is unity. As  $\langle ab \rangle$  and  $\langle \bar{C} \rangle^+$  have the same dependence with respect to the Schmidt number, the ratio  $\langle ab \rangle / (\partial \langle \bar{C} \rangle^+ / \partial y^+)$  depends only on the turbulent Reynolds number. This implies that  $\delta_c^+$ , which may be thought of as the dimensionless thickness of the diffusive sublayer, evolves as

$$\delta_c^+ = f(Re)Sc^{-1/2}. \quad (4)$$

The result (4) is not new and has been derived by several authors (e.g. Coantic 1986; Brumley & Jirka 1988). However, the usual derivation is either based on qualitative scaling arguments or, in eddy-diffusivity models, makes use of the ratio of the turbulent diffusivity and eddy viscosity, whereas the latter can only be defined in the presence of a mean velocity gradient. The present derivation indicates that the same result can be obtained by a reasoning entirely based on the properties of the mean and fluctuating concentration and of the normal velocity fluctuation within the diffusive sublayer.

As (4) shows that  $\delta_c^+ Sc^{1/2}$  depends only on the turbulent Reynolds number, we conclude that the length scale we seek is  $y^+ Sc^{1/2} = yu / (\nu D)^{1/2}$ , which is a mixed length scale involving both the kinematic viscosity and the molecular diffusivity. Hence, if our reasoning is correct, when plotted *vs.*  $y^+ Sc^{1/2}$ , the near-surface profiles of all statistical quantities involving in some way the turbulent mass flux should collapse on a single curve, irrespective of the value of the Schmidt number. The following subsections will prove that this statement is correct.

### 3.2. Mean concentration

The near-surface profiles of the dimensionless mean concentration  $(1 - \langle \bar{C} \rangle) / \Delta C$  are plotted in figure 1 for the four Schmidt numbers  $Sc = 1, 10, 100$  and  $200$ . As we expected, all four profiles collapse onto a single curve, the tiny variations about this curve being due to a somewhat marginal statistical convergence. Up to  $Sc^{1/2} y^+ \approx 5.0$  the concentration profile is linear, clearly defining a diffusive sublayer (frequently hereinafter referred to as the inner diffusive sublayer). In this region, figure 1 indicates  $(1 - \langle \bar{C} \rangle) / \Delta C \approx 0.072 Sc^{1/2} y^+$ . The prefactor 0.072 is of course  $Re$ -dependent and will be shown to be closely related to the mass transfer rate in §5. Note that in contrast with the usual near-wall situation, the viscous sublayer attached to the surface is much thicker than the diffusive sublayer corresponding to  $Sc = 1$ , as in CM (§5.1) it was found that the thickness of the viscous sublayer is about 18 ‘surface’ units, corresponding to  $y/L \approx 2.0 Re^{-1/2}$ . The reason for this is that the concentration and velocity fields experience different surface conditions, one being of Dirichlet type while the other is of Neumann type. It is also important to notice that the Kolmogorov sublayer, i.e. the thin subsurface region where the normal velocity grows linearly with  $y$ , extends up to  $y^+ \approx 8.5$ , i.e.  $y/L \approx 4.0 Re^{-3/4}$ . Hence, we see that when expressed

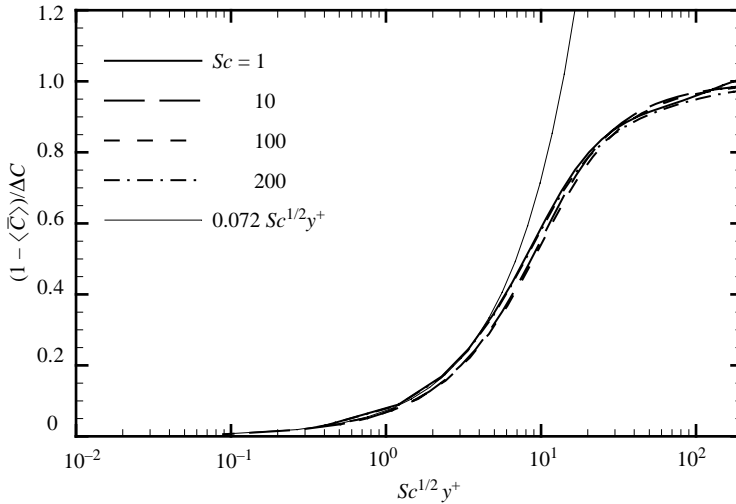


FIGURE 1. Mean concentration profiles  $(1 - \overline{C})/\Delta C$  in the near-surface region.

in  $Sc^{1/2}y^+$  units, the thickness  $\delta_c$  of the diffusive sublayer is about half that of the Kolmogorov sublayer at the present Reynolds number. In other terms we are suggesting that  $\delta_c/L \approx 2.0Re^{-3/4}Sc^{-1/2}$ , i.e. that the above diffusive sublayer can be identified with the Batchelor sublayer  $\delta_B$  defined by Brumley & Jirka (1988). Indeed, given the present Reynolds number  $Re \approx 360$ , if  $\delta_c$  were scaling as  $Re^{-1/2}Sc^{-1/2}$ ,  $Sc^{1/2}\delta_c^+$  should be close to 18 rather than 5. To confirm that  $\delta_c/L$  scales with  $Re^{-3/4}$  we also use the data provided by Yamamoto *et al.* (2001) who computed mass transfer in an open-channel flow at a Reynolds number of 200 based on the friction velocity  $u^*$  and total depth  $2\delta$ . According to the profile of the r.m.s. velocity fluctuations displayed in their figure 3, we estimate that the surface-influenced region extends over a distance  $L \approx 0.6\delta$ , while the kinetic energy at  $y=L$  yields  $u \approx 0.88u^*$ , resulting in  $Re \approx 105$ . Moreover their comment indicates that for  $Sc=1$  they observe a linear profile of the mean concentration up to  $yu^*/\nu = 4.2$ , i.e.  $\delta_c^+ \approx 3.7$ . Since the above scaling suggests that  $\delta_c^+$  should evolve as  $Re^{1/4}$  for a given Schmidt number, we should have  $\delta_c^+ \approx 5.0$  for  $Re=360$ , which is indeed what we found in figure 1. Although the two Reynolds numbers are not widely separated, this is another indication that the above scaling is correct (if  $\delta_c/L$  were scaling with  $Re^{-1/2}$ , the value obtained by Yamamoto *et al.* (2001) should result in  $\delta_c^+ \approx 6.9$  for  $Re=360$ , which is clearly larger than what is displayed by figure 1). Hence the combination of present results obtained over a wide range of  $Sc$  but at a single  $Re$  with those of a DNS study where  $Re$  is 3.5 times smaller, strongly supports the conclusion that the layer throughout which the mean concentration profile evolves linearly may be identified with the Batchelor sublayer  $\delta_B$ . An illustration of the relative position of the various sublayers at the present turbulent Reynolds number  $Re=360$  is given in figure 2 for  $Sc=10$ .

The diffusive sublayer is followed by a buffer layer where the mean concentration varies rapidly. Farther from the surface and for high enough turbulent Péclet numbers ( $Pe = ScRe$ ), classical arguments (Monin & Yaglom 1973, § 5.7; Yaglom & Kader 1974) imply the existence of an intermediate region within which the mean concentration profile obeys a logarithmic law of the form  $(1 - \overline{C})/c = A \ln y^+ + B$ ,  $A$  and  $B$  being two ‘universal’ constants. This region is easily detected on the right-hand side of figure 1, typically for  $Sc^{1/2}y^+ > 40$ . However the two constants are  $Sc$ -dependent in

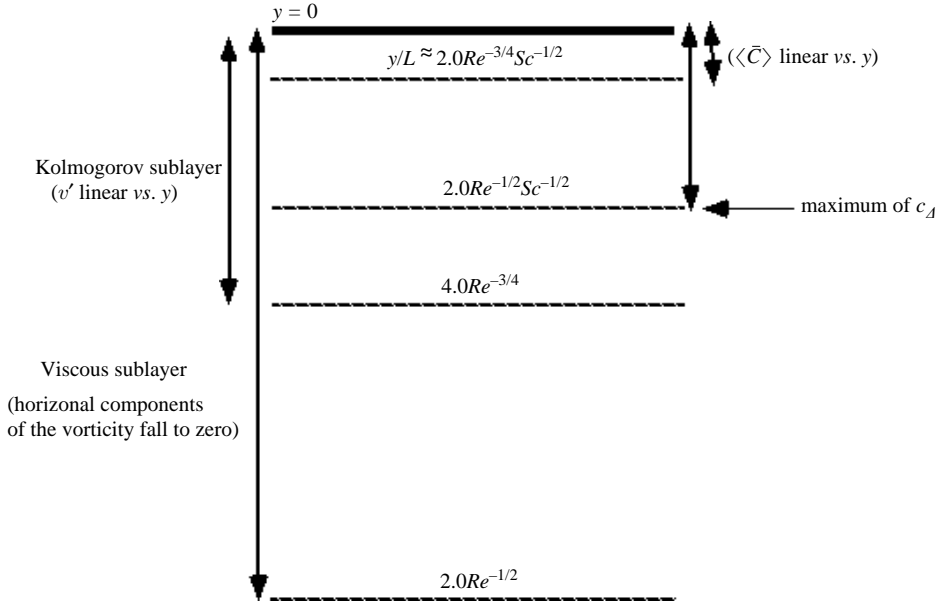


FIGURE 2. The various viscous and diffusive sublayers below the surface for  $Re = 360$  and  $Sc = 10$ . Note that for  $Sc < 5$ , the outer diffusive layer becomes thicker than the Kolmogorov sublayer. The dynamically surface-influenced region extends up to  $y/L \approx 1$ , i.e. it is about ten times thicker than the viscous sublayer.

the  $((1 - \langle \bar{C} \rangle)/\Delta C, Sc^{1/2}y^+)$  representation. This makes it clear that the length scale  $Sc^{1/2}y^+$  is only appropriate close to the surface, whereas  $(1 - \langle \bar{C} \rangle)/\Delta C$  is necessarily  $Sc$ -dependent in the bulk because the molecular diffusivity no longer plays a role. In the core of the flow (not shown here), the mean concentration becomes a linear function of the distance to the surface. Given the negligible value of the first term on the left-hand side of (3) in this region, this indicates that, far enough from the surface, the turbulent diffusivity is constant, as we expect in a high-Reynolds-number, almost homogeneous, turbulent flow.

### 3.3. Second-order statistics

Figure 3 shows the vertical profiles of the r.m.s. concentration fluctuation  $c_\Delta = \langle c''^2 \rangle^{1/2}/\Delta C$  over a region corresponding to one integral length scale. All profiles indicate that the absolute maximum of the r.m.s. fluctuation is reached very close to the surface; the higher the Schmidt number, the closer to the surface the location of this maximum. The values of the maximum of  $c_\Delta$  are found to depend only weakly on the Schmidt number, which indicates that they are mostly determined by the turbulence intensity. In contrast, while  $c_\Delta$  keeps a significant magnitude in the bulk for  $Sc = 1$ , it is almost zero out of the near-surface region for the other three Schmidt numbers. This reflects the fact that for high Schmidt numbers, the resistance to the transfer is essentially located in the diffusive sublayer, while the small amount of dissolved gas that succeeds in crossing this sublayer is then quickly mixed in the bulk.

We can of course wonder whether this decrease of  $c_\Delta$  as  $y$  increases is not due in good part to the increase of the vertical grid spacing  $\Delta y$ . Indeed, as the grid becomes coarser, the unresolved part of the concentration fluctuation increases. However, it may be shown that the relative contribution of scalar structures smaller than the Kolmogorov microscale (those belonging to the so-called viscous-convective

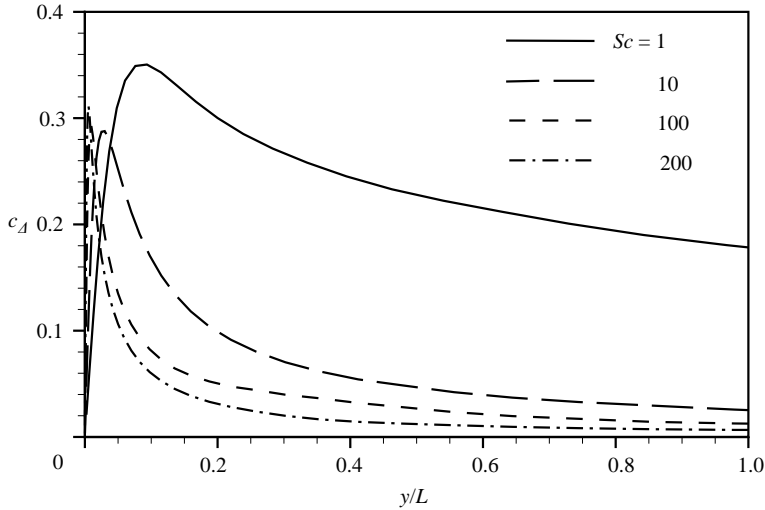


FIGURE 3. Resolvable r.m.s. concentration fluctuations  $c_{\Delta} = \langle c''^2 \rangle^{1/2} / \Delta C$  in the upper part of the flow.

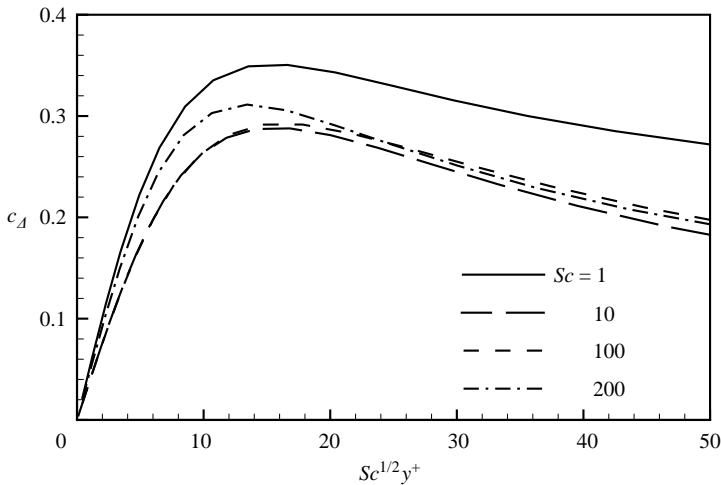


FIGURE 4. Resolvable r.m.s. concentration fluctuations  $c_{\Delta}$  in the near-surface region.

subrange) is of  $O(Re^{-1/2} \log(Sc))$ . Hence they only provide a small correction to the total variance. Similarly, the contribution of structures whose size is between the Kolmogorov microscale and the cutoff length scale  $\Delta y$  is of  $O((\Delta y/L)^{2/3})$ , provided the cutoff lies within the inertial subrange. As the present grid is such that  $\Delta y$  is still about 3.3 (resp. 6.5) Kolmogorov microscales for  $y/L=0.5$  (resp. 1.0), these unresolved contributions are small throughout the near-surface region. Hence we can conclude that, provided the mechanisms that generate the concentration fluctuation are properly captured (this will be shown to be the case in §3.4), the grid is able to predict properly the magnitude of the total r.m.s. concentration throughout the near-surface region  $y/L < 1$ .

The behaviour of the r.m.s. fluctuations in the near-surface region are seen in more detail in figure 4. This figure confirms the relevance of the scaling derived in §3.1,

as the maximum of  $c_\Delta$  is reached around  $Sc^{1/2}y^+ = 15$  whatever the value of  $Sc$ . In other terms, figure 4 shows that for a given  $Re$ , the location of this maximum evolves as  $Sc^{-1/2}$ . Moreover, having noticed that at the present Reynolds number the viscous sublayer extends up to  $y^+ \approx 18$  which corresponds to  $y/L \approx 2.0Re^{-1/2}$ , we infer that  $c_\Delta$  reaches its maximum at a distance  $\delta_D \approx 2.0Re^{-1/2}Sc^{-1/2}$ , i.e.  $2.0Pe^{-1/2}$ . This value of  $\delta_D$  corresponds to the thickness of the ‘outer diffusive sublayer’ identified by Brumley & Jirka (1988). This outer diffusive layer is indicated in figure 2; note that with the moderate value of the turbulent Reynolds number considered here,  $\delta_D$  is less than the thickness of the Kolmogorov sublayer for  $Sc > 5$ . The  $Re^{-1/2}$  scaling suggested above may be confirmed by using the low- $Re$  DNS results of Handler *et al.* (1999) ( $Sc = 2$ ,  $Re \approx 95$ ). They mention that the r.m.s. concentration fluctuation reaches a maximum at  $yu^*/\nu = 8$ , i.e.  $yu/\nu \approx 7.0$  ( $u \approx 0.88u^*$  in their case). As their figure 5 indicates that the horizontal vorticity fluctuations start to be affected by the shear-free condition at  $yu^*/\nu \approx 11$ , we deduce that the viscous sublayer has a dimensionless thickness  $\delta_{\nu u}/\nu \approx 10$  in their case. Hence we conclude that  $\delta_{Du}/\nu = \delta_{\nu u}/\nu Sc^{-1/2} \approx 7.0$ , which confirms that the r.m.s. concentration reaches its maximum at  $y \approx \delta_D$ .

The maximum value of  $c_\Delta$  is only slightly  $Sc$ -dependent and lies in the range 0.31–0.35 (the two cases  $Sc = 10$  and 100 are somewhat poorly converged, so that the slightly lower value of the corresponding maxima and the crossing of the corresponding curves with those for  $Sc = 1$  and 200 are certainly meaningless). These values may be compared with those obtained in low- $Re$  open-channel DNS by Handler *et al.* (1999) ( $Sc = 2$ ,  $Re^* = 180$ ) and Yamamoto *et al.* (2001) ( $Sc = 1$  and 5,  $Re^* = 200$ ). After evaluating  $L$  and  $\Delta C$  in both groups of simulations, it turns out that the maximum of  $c_\Delta$  is always in the range 0.33–0.35, which confirms present findings. Recent experimental results obtained by Atmane & George (2002) in a grid-stirred tank using an oxygen microprobe also indicate a maximum of  $c_\Delta$  about 0.30. The slope of the  $c_\Delta$ -profiles right at the surface does not depend on  $Sc$  as will be shown below, which confirms that  $Sc^{1/2}\nu/u$  and  $\Delta C$  are indeed the correct length and concentration scales describing the vertical variations of the r.m.s. concentration fluctuation very close to the surface. However, figure 4 reveals that the profiles of  $c_\Delta$  remain  $Sc$ -dependent over most of the near-surface region, even when plotted against  $Sc^{1/2}y^+$ , which indicates that the r.m.s. concentration fluctuation depends in a complex way on the above scales as well as on the scales  $L$  and  $c$ . This contrasts with the behaviour of the mean concentration for which figure 1 indicates that the effect of the outer length scale occurs only at larger distances from the surface, typically for  $Sc^{1/2}y^+ > 80$ . This suggests that the evolution of the concentration fluctuations and those of the mean concentration are not affected in the same way by molecular diffusion.

Figure 5 displays the asymptotic behaviour of  $c_\Delta$  and  $(cv)^+ = \langle c''v'' \rangle / uc$  as  $Sc^{1/2}y^+ \rightarrow 0$  for the two extreme Schmidt numbers  $Sc = 1$  and 200. In agreement with the expansions established in §3.1,  $c_\Delta$  is found to evolve linearly with  $Sc^{1/2}y^+$  in the top part of the diffusive sublayer, while the resolved turbulent flux exhibits a quadratic behaviour. The normalization of concentration fluctuations by  $\Delta C$  and that of turbulent fluxes by  $cu$  is found to produce  $Sc$ -independent values of the ratios  $c_\Delta/Sc^{1/2}y^+$  and  $(cv)^+/Scy^{+2}$  (as the magnitude of the subgrid terms increases with the Schmidt number, these terms result in a slightly smaller magnitude of the resolved quantities for  $Sc = 200$ , as compared with those corresponding to  $Sc = 1$ ). Present calculations yield the asymptotic values  $c_\Delta/Sc^{1/2}y^+ \approx 0.052$  and  $(cv)^+/Scy^{+2} \approx 8.3 \cdot 10^{-3}$ . An improved estimate of the turbulent flux may be obtained by adding the subgrid terms, i.e. the Leonard and modelled fluxes, to the resolved flux. As shown in figure 6, the Leonard flux (second and third terms on the right-hand side of (2)

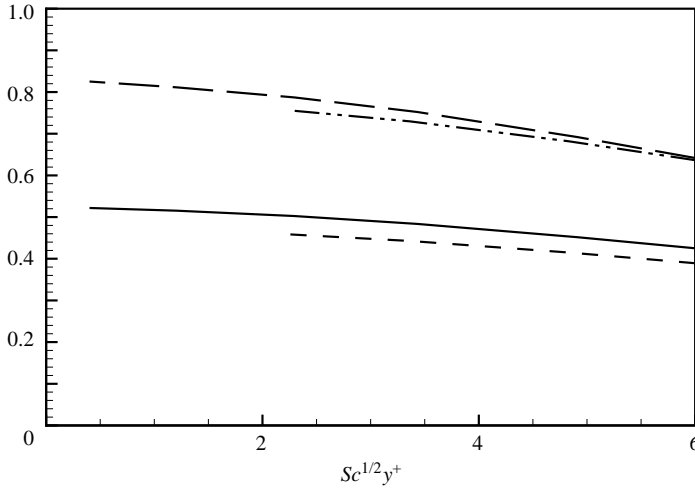


FIGURE 5. Asymptotic behaviours of the r.m.s. concentration fluctuation and turbulent flux near the surface.  $Sc = 1$ : —,  $10c_{\Delta}/Sc^{-}y^+$ ; - - -,  $100(cv)^+/Scy^{+2}$ .  $Sc = 200$ : - - -,  $10c_{\Delta}/Sc^{-}y^+$ ; - · - · -,  $100(cv)^+/Scy^{+2}$ .

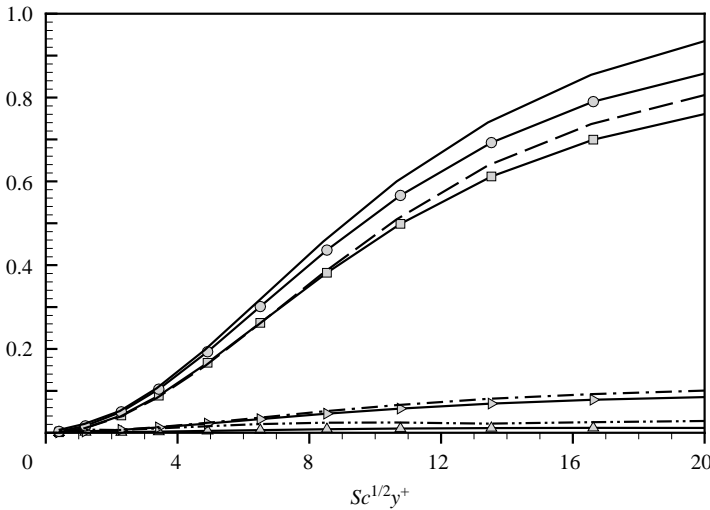


FIGURE 6. Turbulent mass flux in the vicinity of the surface (all terms are normalized by  $uc$ ). Resolvable flux  $\langle c''v'' \rangle$ : - - -,  $Sc = 200$ ; —□—,  $Sc = 1$ . Modelled subgrid-scale flux: - · - · -,  $Sc = 200$ ; —△—,  $Sc = 1$ . Leonard flux: —·—,  $Sc = 200$ ; —○—,  $Sc = 1$ . Total turbulent flux: —,  $Sc = 200$ ; —○—,  $Sc = 1$ .

for  $i = 2$ ) contributes about 15% in the total flux at a distance  $Sc^{1/2}y^+ \approx 20$  from the surface for both Schmidt numbers. The modelled flux (first term on the right-hand side of (2)) remains significantly smaller in both cases. The relative contribution of the subgrid-scale terms increases as the surface is approached and reaches 32% (resp. 40%) at the grid point closest to the surface for  $Sc = 1$  (resp. 200). If these subgrid-scale terms are added to the resolved flux, the limit behaviour of the total turbulent flux  $\langle c''v'' + q_2 \rangle^+$  is found to be  $0.011Scy^{+2}$  for both Schmidt numbers. The above results for  $c_{\Delta}$  and  $(cv)^+$  may be used to compare the surface value of

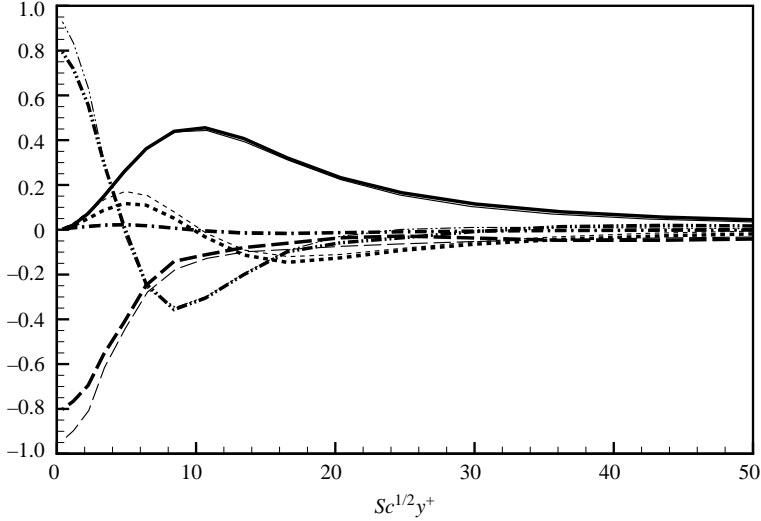


FIGURE 7. Budget of  $\langle c'^2 \rangle$  in the near-surface region (all terms are normalized by  $(cu)/D$ . —, production  $P_c$ ; — —, turbulent transport  $T_c$ ; - - -, cascade term  $TL_c$ ; - · - ·, diffusion  $D_c$ ; · · ·, dissipation  $\varepsilon_c$ .  $Sc = 1$  (thin lines);  $Sc = 200$  (thick lines).

the correlation coefficient  $(cv)^+/c^+v^+$  (with  $c^+ = (\Delta C/c)c_\Delta$  and  $v^+ = \langle v'^2 \rangle^{1/2}/u$ ) with that obtained in the DNS of Nagaosa (1999) at a Reynolds number roughly 5 times smaller than the present one. Using the asymptotic behaviour of the normal velocity fluctuation reported in CM, i.e.  $v^+/y^+ \approx 1.51 \cdot 10^{-2}$  (in the present normalization), we find  $(cv)^+/c^+v^+ \approx 0.77$  at the surface, in good agreement with the value 0.74 reported by Nagaosa.

### 3.4. Budget of the concentration variance

Let us now examine the budget of the resolved variance  $\langle c'^2 \rangle$ . As the flow and the concentration field are statistically stationary and periodic in the  $x$ - and  $z$ -directions, this budget reduces to

$$0 = -2\langle c''v'' \rangle \frac{d\langle \bar{C} \rangle}{dy} + \varepsilon_c + \frac{d}{dy} \left[ -\langle c'^2 v'' \rangle - 2\langle L''_c c'' \rangle + \langle D + D_T \rangle \frac{d\langle c'^2 \rangle}{dy} \right], \quad (5)$$

where the scalar ‘dissipation’  $\varepsilon_c$  is dominated by the term  $-2\langle (D + D_T)(\partial c''/\partial x_k)^2 \rangle$  but also comprises additional secondary contributions resulting from the fluctuations of the Leonard flux and subgrid-scale diffusivity (Calmet & Magnaudet 1997). The other terms on the right-hand side of (5) represent production of  $\langle c'^2 \rangle$  by the mean concentration gradient ( $P_c$ ), turbulent transport by the resolved normal velocity fluctuation ( $T_c$ ), transport by the largest unresolved normal velocity fluctuation ( $TL_c$ ), and diffusion ( $D_c$ ). The various terms in (5), normalized by  $(uc)^2/D$ , are plotted in figure 7 for  $Sc = 1$  and  $Sc = 200$  vs. the normalized distance  $Sc^{1/2}y^+$ . The profiles of all terms are seen to collapse nicely on  $Sc$ -independent curves, up to small differences due to the subgrid-scale contributions.

All terms in these budgets go to zero at the surface, except dissipation and viscous diffusion which reach their maximum there and balance each other. These behaviours agree with the Taylor expansions near  $y^+ = 0$  by which we find that  $P_c$ ,  $T_c$  and  $TL_c$  decay like  $y^{+2}$  near the surface. The production term is positive everywhere. As  $d\langle \bar{C} \rangle/dy$  is negative, this indicates that  $\langle c''v'' \rangle$  is positive, which may be interpreted

as the fact that  $\langle c''v'' \rangle$  is dominated by contributions corresponding to the first ( $v'' > 0, c'' > 0$ ) and third ( $v'' < 0, c'' < 0$ ) quadrants. This is because downwelling (resp. upwelling) motions essentially carry blobs of fluids whose concentration in contaminant is higher (resp. lower) than the local mean because they come from the surface (resp. bulk) region where  $C$  is maximum (resp. minimum). In contrast, the transport term  $T_c$  changes sign very close to the surface, at a location  $y_m$  such that  $Sc^{1/2}y_mu/\nu \approx 10$ . For  $y < y_m$ , the transport term is positive because upwelling motions tend to increase the local concentration variance by bringing large concentration fluctuations produced in the region where the r.m.s. concentration fluctuation reaches its maximum ( $Sc^{1/2}y^+ \approx 15$ ). Similarly, for  $y > y_m$ ,  $T_c$  is negative because these large concentration fluctuations are brought there by downwelling motions. This behaviour is directly reflected in the skewness factors of  $c''$  and  $v''$  (not shown). Indeed, the skewness factor of  $v''$  is negative everywhere (keeping in mind that the  $y$ -axis is directed downwards) whereas that of  $c''$  is found to be negative only for  $Sc^{1/2}y^+ < 15$ , approximately, i.e. within the outer diffusive layer (the surface values of the skewness factor  $S(c'')$  are about  $-1.0$ ). Hence, as already noticed by Handler *et al.* (1999), it appears that the strongest concentration fluctuations are associated with the strongest vertical velocity fluctuations (upwellings) only within a very thin layer of fluid below the surface, which we may roughly identify with the outer diffusive sublayer.

Four main near-surface regions may be observed in the budget (5). Far enough from the surface (typically for  $Sc^{1/2}y^+ > 45$ ), dissipation and production are essentially in balance. Then there is an intermediate region (typically  $20 < Sc^{1/2}y^+ < 45$ ) where turbulent transport and dissipation act together to balance production. The third region ( $3.5 < Sc^{1/2}y^+ < 20$ ) is that located about the broad maximum of  $\langle c''^2 \rangle$ . This is also the region where  $P_c$  reaches its maximum ( $P_{cmax} \approx 0.45$ ) and where  $T_c$  changes sign. Since the profile of  $\langle c''^2 \rangle$  exhibits a significant negative curvature in this zone, the diffusion term takes negative values which, together with the dissipation term, balance the large positive values of  $P_c$ . In the fourth region, very close to the surface,  $P_c$  and  $T_c$  become negligibly small and the large negative values of  $\varepsilon_c$  are balanced by the diffusion term  $D_c$  which has changed sign and reaches large positive values because of the rapid quadratic growth of  $\langle c''^2 \rangle$  with the distance to the surface.

Note that as  $\langle c''v'' \rangle$  is constant throughout the flow outside the outer diffusive layer (see (3)), its value at large  $Sc^{1/2}y^+$  is entirely determined by the processes that take place in the top part of this thin layer. Hence, provided this crucial region is accurately described by the computational grid (which we expect to be the case because the grid is fine enough there for the LES to be locally a DNS in the vertical direction), the value of the production term  $P_c$  is properly predicted throughout the flow (there is no doubt that even though  $\Delta y$  increases with the distance to the surface, the grid remains everywhere capable of capturing the small mean concentration gradient that subsists below the outer diffusive layer). As we saw above that, for large  $Sc^{1/2}y^+$ , the concentration variance is controlled by the local value of  $P_c$ , we conclude that the rate at which this variance is produced is correctly predicted whatever the distance to the surface. Combined with the comment made at the beginning of §3.2, this makes us confident that the values of the resolved r.m.s. concentration predicted by the present LES approach provide realistic estimates of the total r.m.s. concentration throughout the entire near-surface region.

To conclude this analysis, it is worth comparing the maximum intensity of the r.m.s. concentration fluctuations near a free surface with its near-wall counterpart. As shown in figure 2,  $c_\Delta$  reaches a maximum of about 0.35 near the surface, whereas the maximum found near the bottom wall (not shown) is about 0.20 when normalized in

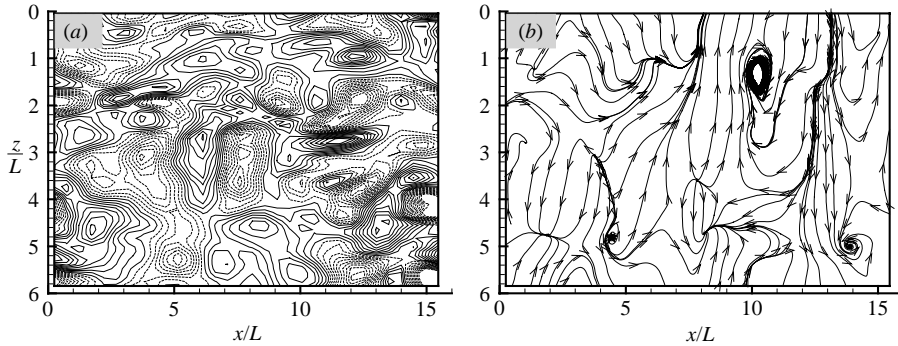


FIGURE 8. (a) Iso-contours of the normal velocity fluctuation in the plane  $y^+ = 0.07$  (from  $-10^{-4}$  to  $10^{-4}$  with an increment of  $10^{-5}$ ). Negative values: dashed lines; positive values: solid lines. (b) Instantaneous streamlines on the surface.

the same manner. The reason for this difference may be understood by evaluating the ratio  $\varepsilon_c/P_c$ . In the former case this ratio is about 0.3 in the region of the maximum, while it is about 0.6 in the latter case. The absence of shear near the free surface results in a smaller number of dissipative small-scale structures (Hunt 1984) and hence in a lower value of the ratio  $\varepsilon_c/P_c$ , which in turn allows the concentration fluctuations to reach higher values.

#### 4. Relationship between the near-surface concentration and velocity fields

The most widely accepted conclusion of the numerous available investigations devoted to mass transfer across a shear-free interface is probably the validity of the concept of surface renewal (Highbie 1935; Dankwerts 1951), remarkably supported by the measurements of Komori, Murakami & Ueda (1989). In this section, we try to provide further information on the connection between the mass transfer process and the structure of the underlying turbulence by examining the spatial relationship between the resolved concentration field and the velocity fluctuations in the near-surface region.

In open-channel flows, as well as in grid-stirred tanks, near-surface dynamics are dominated by ‘patchy’ structures, i.e. large-scale structures without any preferential orientation. In both cases, the upwelling structures (frequently referred to as updraughts or splats) result from the ejection of fluid blobs from the bottom part of the flow (see e.g. Komori *et al.* 1989 for a discussion of the connection with the bursting process in the case of small-depth open-channel flow). The vanishing of the vertical velocity at the surface then forces updraughts to stretch in the horizontal directions and roll up, resulting in the creation of downwelling structures (also referred to as downdraughts or antisplats) when two neighbouring updraughts collide (Perot & Moin 1995). Iso-contours of the upwelling ( $v'' < 0$ ) and downwelling ( $v'' > 0$ ) motions very close to the surface are shown in figure 8(a). Not surprisingly, the typical horizontal size of these structures is found to be about  $2L$ , corresponding to the turbulence macroscale (Tennekes & Lumley 1972, p. 273). The presence of upwelling and downwelling large-scale motions in the immediate vicinity of the surface results in complex displacements of fluid elements right at the surface. An instantaneous view of the large-scale surface streamlines taken at the same time as the normal velocity field of figure 8(a) is shown in figure 8(b). As may be expected,

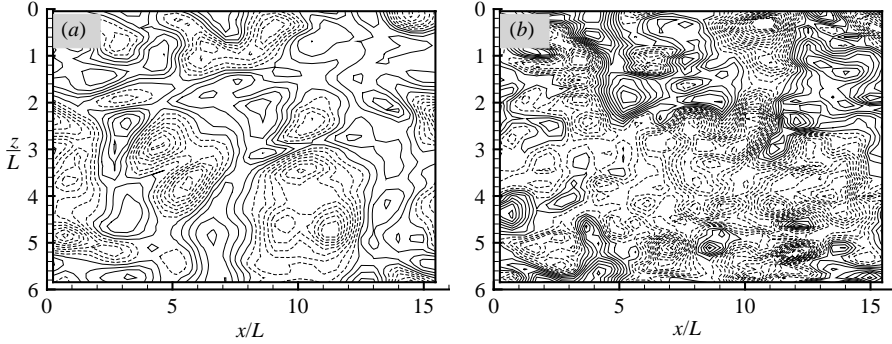


FIGURE 9. Iso-contours of  $c''$  in two horizontal planes ( $Sc = 1$ ). (a)  $y^+ \approx 1.2$  (from  $-0.12$  to  $0.05$  with an increment of  $0.01$ ); (b)  $y^+ \approx 100$  (from  $-0.15$  to  $0.1$  with an increment of  $0.01$ ). Negative values: dashed lines; positive values: solid lines.

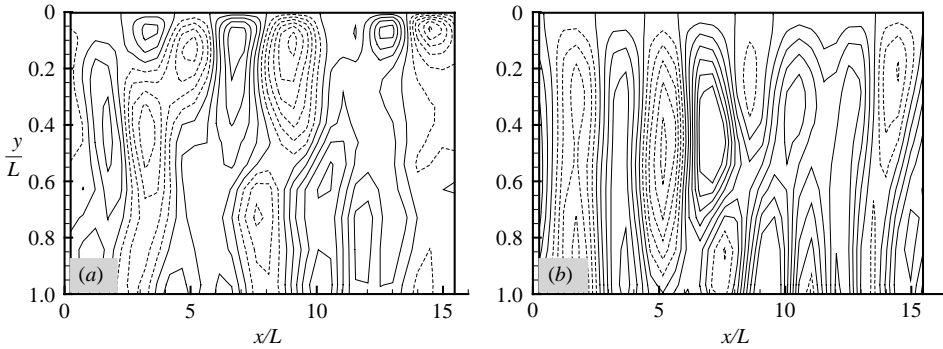


FIGURE 10. Iso-contours of  $v''$  and  $c''$  ( $Sc = 1$ ) in the near-surface part of a vertical plane. (a)  $c''$  (from  $-0.3$  to  $0.2$  with an increment of  $0.05$ ); (b)  $v''$  (from  $-0.04$  to  $0.03$  with an increment of  $0.005$ ). Negative values: dashed lines; positive values: solid lines.

upwelling (resp. downwelling) motions in figure 8(a) are found to correspond to sources (resp. sinks) in figure 8(b). Within the Kolmogorov sublayer described in §3.2, we may write  $v''|_y \approx (\partial v'' / \partial y)|_y = -(\nabla_S \cdot \mathbf{v}_S)y$ , where  $\nabla_S \cdot \mathbf{v}_S$  stands for the so-called surface divergence of the instantaneous velocity. In other words, figure 8(a) provides an instantaneous representation of the horizontal dilation/compression rate of the surface velocity field. Figure 9 shows some iso-contours of  $c''$  for  $Sc = 1$  in two horizontal planes, one located within the diffusive sublayer ( $y^+ \approx 1.2$ ), the other in the log-layer of the mean concentration profile ( $y^+ \approx 100$ ). The largest concentration fluctuations in the plane  $y^+ \approx 1.2$  are seen to be negative, corresponding to the action of upwelling motions, but such events are rare and most of the surface in this plane is occupied by small positive fluctuations associated with downwelling motions that drive the contaminant towards the bulk. In contrast, a larger fraction of the surface corresponds to negative values of  $c''$  in the plane located farther from the surface, suggesting that the mixing process there is mostly governed by the upwelling motions which are statistically more vigorous than the downwelling motions. A vertical cross-section of  $c''$  (for  $Sc = 1$ ) and  $v''$  throughout the near-surface region is shown in figure 10. This plot reveals a succession of high- and low-concentration structures with various vertical sizes. Not surprisingly, comparison of figure 10(a) with the snapshot of the vertical velocity fluctuations (figure 10(b)) shows that upwelling (resp.

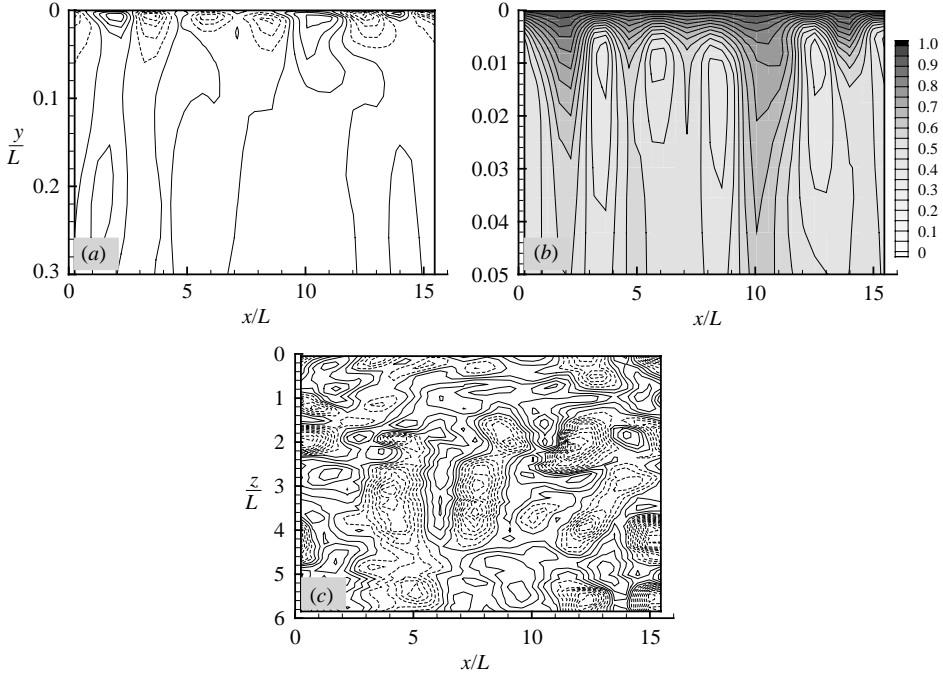


FIGURE 11. Near-surface iso-contours of the concentration for  $Sc=200$ . (a)  $c''$  in a vertical plane (from  $-0.3$  to  $0.2$  with an increment of  $0.05$ ); (b) instantaneous concentration  $c'' + \overline{c}$  in the same plane; (c)  $c''$  in the horizontal plane  $y^+ \approx 0.07$  (from  $-0.12$  to  $0.05$  with an increment of  $0.01$ ). Negative values: dashed lines; positive values: solid lines.

downwelling) motions contribute to low (resp. high) concentration. The maximum values of  $c''$  arise around  $y=0.1L$ , i.e.  $y^+=18$ , in line with figure 4. In this region, the upwelling structures have more energy than the downwelling ones, so that the turbulent flux  $\langle c''v'' \rangle$  is dominated by the contribution of upwelling motions carrying low-concentration fluid (third quadrant). A vertical cross-section of the iso-contours of  $c''$  at  $Sc=200$  is provided in figure 11(a). The concentration patches now extend over a much thinner layer whose typical thickness is about  $0.04L$ , i.e. ten surface units. The instantaneous concentration field corresponding to figure 11(a) is shown in grey levels in figure 11(b). The diffusive sublayer is clearly visible at the top. Its thickness is seen to undulate slightly, owing to the alternate compression and dilation induced by the updraughts and downdraughts. The high-concentration structures driven by the downdraughts mostly take the form of ‘needles’ that penetrate into the flow interior. These needles represent the dominant large-scale mode by which the pollutant is transferred from the surface towards the bulk. Obviously, this picture only describes the behaviour of structures which are large (typically  $O(L)$ ) in the horizontal direction. Herlina & Jirka (2004) resolved much smaller concentration structures (typically a few per cent of  $L$ ) using an LIF technique. The structures they report look rather like thin layers torn away from the diffusive sublayer when the latter is peeled off by a turbulent eddy, and then stretched and fold by downwelling eddies. For moderate-to-high  $Re$ , there is of course a broad and continuous spectrum of concentration structure sizes and we believe the large-scale structures revealed by the present LES and the small-scale ones detected by the LIF are just two partial and

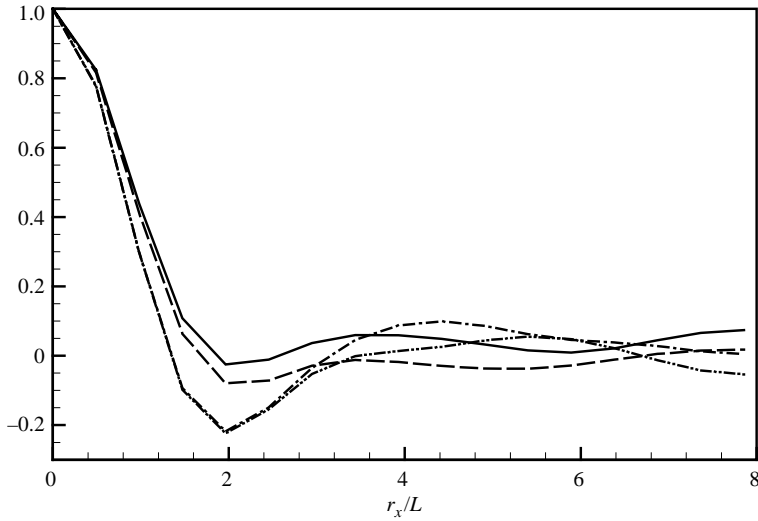


FIGURE 12. Longitudinal two-point correlations: —,  $R_{vv}$  ( $y^+ \approx 1.2$ ); - - -,  $R_{vv}$  ( $y^+ \approx 0.07$ ); — · —,  $R_{cc}$  ( $Sc = 1$  and  $y^+ \approx 1.2$ ); · · ·,  $R_{cc}$  ( $Sc = 200$  and  $y^+ \approx 0.07$ ).

complementary views of a much more complex reality whose complete description is far beyond present computational and experimental capabilities.

Figure 11(c), which corresponds to the same instantaneous concentration field as figures 11(a) and 11(b), shows the iso-concentration structures in the horizontal plane  $y^+ = 0.07$ . In spite of the close vicinity of the surface, patchy structures are clearly visible, with positive and negative values of  $c''$  covering almost the same percentage of the plane. The above snapshots, especially figures 9(a) and 11(c), emphasize the sensitivity of the concentration field to the large-scale dynamics of the turbulent field, even within the diffusive sublayer where molecular effects are dominant. Indeed, the iso-contours of  $c''$  (figure 11c) and those of  $v''$  (figure 8a) at the same distance from the surface just mirror each other, as upwelling structures impinging on the surface carry low concentration fluid and *vice versa*. As we saw that there is a linear relationship between  $v''$  and  $\nabla_s \cdot v_s$  within the Kolmogorov sublayer, we conclude that there is a one-to-one correspondence between the concentration fluctuation and the surface divergence within the diffusive sublayer. Note that in contrast with low- $Re$  investigations where a significant degree of correlation between streamwise or spanwise vorticity and near-surface concentration was observed (Komori *et al.* 1993; Handler *et al.* 1999; Nagaosa 1999), no such feature was noticed here. This suggests that such strong correlations are a distinctive feature of low- $Re$  open-channel flows where most of the bursts emanating from the bottom boundary layer interact directly with the surface, whereas at high enough Reynolds number, the two regions are more widely separated and the only dynamical quantity with which the near-surface scalar field correlates well is the vertical velocity.

Figure 12 shows two-point streamwise correlation coefficients of the normal velocity fluctuation ( $R_{vv}$ ) and concentration fluctuation ( $R_{cc}$ ) at the same vertical location and for the same Schmidt numbers as in figures 9(a) and 11. In both cases, it turns out that the profiles of  $R_{cc}$  and  $R_{vv}$  are very similar. In particular, both curves reach a negative minimum for a separation distance  $r_x/L$  of about 2, corresponding to the macroscale  $2L$ . Indeed, this distance represents the separation between two neighbouring zones where the vertical velocities have opposite signs. The minimum of  $R_{vv}$  and  $R_{cc}$  is

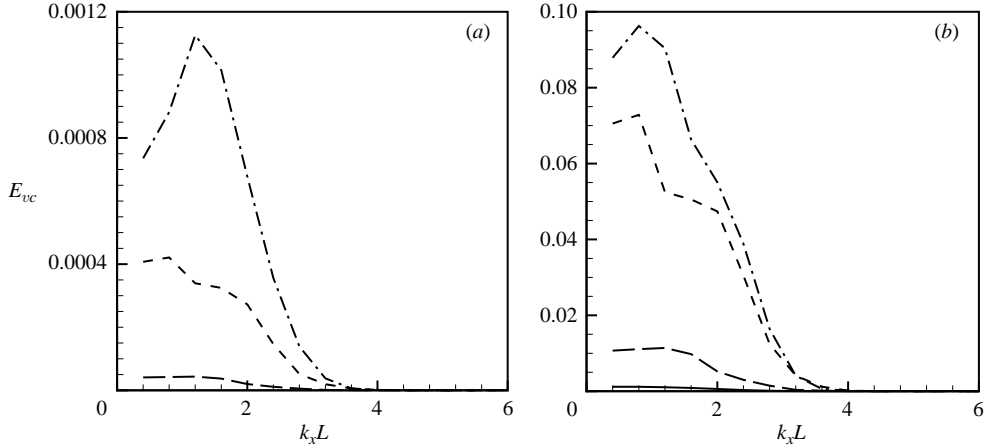


FIGURE 13. Longitudinal co-spectra of  $c''$  and  $v''$ : (a)  $y^+ \approx 0.07$ ; (b)  $y^+ \approx 1.2$ . —,  $Sc = 1$ ; — —,  $Sc = 10$ ; - - -,  $Sc = 100$ ; - · - ·,  $Sc = 200$ .

much more prominent in the plane located closer to the surface ( $y^+ \approx 0.07$ ), where downwelling structures are generated by the impingement of the upwelling ones on the surface. As expected from the comparison of figures 8 and 11, the profile of  $R_{cc}(Sc = 200)$  very closely follows that of  $R_{vv}$  up to  $r_x/L = 3$ , which reflects the fact that molecular diffusion plays almost no role in the structure of the large-scale concentration field at such a high Schmidt number. In contrast,  $R_{cc}(Sc = 1)$  exhibits some differences with  $R_{vv}$  for  $r_x/L > 1$ , making the effect of molecular diffusion more apparent.

The correlation between concentration and normal velocity fluctuations may also be investigated by examining the co-spectrum of these two quantities. The normalized streamwise co-spectrum  $E_{vc}$  is defined as

$$E_{vc}(y, k_x) = \frac{1}{L_x} \text{Re} \left\{ \int_{-L_x/2}^{+L_x/2} \langle v^+(x, y, z, t) c^+(x + r_x, y, z, t) \rangle \exp(-ik_x r_x dr_x) \right\}, \quad (6)$$

where  $\text{Re}$  denotes the real part of the expression and  $L_x$  is the length of the computational domain in the  $x$ -direction. Figure 13 shows  $E_{vc}$  at two different locations  $y^+ \approx 0.07$  and  $y^+ \approx 1.2$  for various Schmidt numbers between 1 and 200. At both locations, it is clearly seen that the higher the Schmidt number, the stronger the correlation between the velocity and the concentration fluctuations, which illustrates how the sensitivity of the mass transfer process increases with  $Sc$ . More precisely, it may be observed that for  $y^+ \approx 0.07$  (which lies within the diffusive sublayer for all the reported values of  $Sc$ ), the maximum of  $E_{vc}$  grows almost linearly with  $Sc$ , which is in line with the linear dependence of  $c^+$  with respect to  $Sc$  within the inner diffusive sublayer (see §3.1). The increase of the maximum of  $E_{vc}$  with  $Sc$  is still observed for  $y^+ \approx 1.2$  but it does not follow a linear trend any more. This is because  $y^+ \approx 1.2$  lies within the diffusive sublayer only for  $Sc = 1$ , while it lies within the buffer layer of the concentration field for both  $Sc = 10$  and 100.

The evolution of  $E_{vc}$  with  $k_x$  also deserves some comments, although the low-wavenumber part of these one-dimensional co-spectra is obviously contaminated by aliasing effects. First, it is apparent that the magnitude of  $E_{vc}$  reaches a maximum or a plateau for  $k_x L \leq 1.5$ , i.e. for separation distances larger than  $4L$ , approximately. As the distance  $\lambda_x$  separating two neighbouring updraughts or downdraughts is

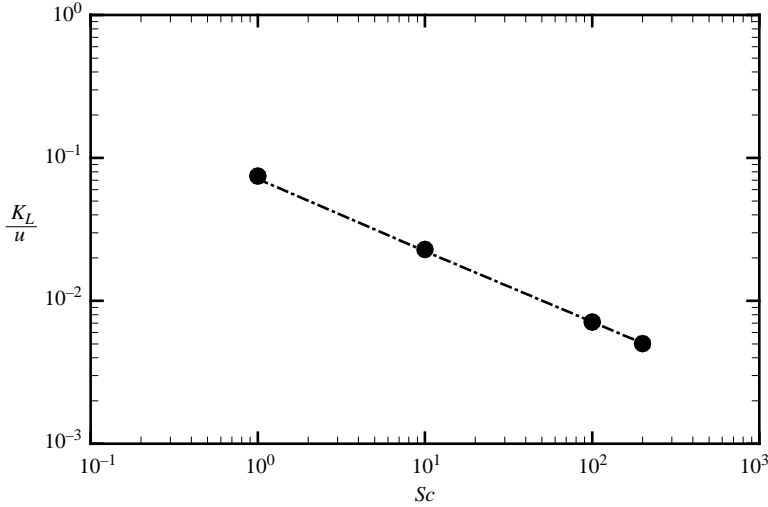


FIGURE 14. Averaged mass transfer coefficient. ●, present study; - · -,  $0.072 Sc^{-1/2}$ .

approximately  $4L$ , the two-point correlation between  $c''$  and  $v''$  is indeed expected to be positive for separations of the order of  $\lambda_x$ . All co-spectra exhibit a sharp negative slope in the range  $1.5 < k_x L < 3.0$ , and there is virtually no contribution of higher wavenumbers. This allows us to draw two conclusions. First, on the technical side,  $k_x L = 3$  is less than the maximum streamwise wavenumber  $(k_x L)_{max} \approx 6.4$  allowed by our computational grid, which makes us confident that the present LES captures all the important features of the mass transfer process. Then, from a physical point of view, the co-spectra of figure 13 emphasize the fact that the integral  $\int_0^\infty E_{vc}(k_x) dk_x$  is dominated by contributions corresponding to wavelengths  $\lambda$  such that  $\lambda \geq \lambda_x$ , i.e. by large-scale structures.

## 5. Mass transfer rate and near-surface hydrodynamics

### 5.1. LES results

The determination and prediction of the average mass transfer rate across a gas–liquid interface has been the subject of a huge literature, as this quantity is a direct measure of the efficiency of the absorption processes that take place at the air–sea interface as well as in many chemical reactors. Although this measure is global, it is frequently the only one accessible to laboratory experiments, since most determinations of the mass transfer efficiency are performed using concentration measurement techniques that only give access to space- and time-averaged concentrations. The mass transfer rate is usually defined as

$$K_L/u_0 = - \frac{D}{u_0 \delta C} \left. \frac{\partial \langle \bar{C} \rangle}{\partial y} \right|_{y=0}, \quad (7a)$$

where  $K_L$  is the so-called mass transfer velocity,  $u_0$  is some characteristic velocity scale and  $\delta C$  is the concentration difference between the surface and the bulk. Setting  $u_0 = u$  and  $\delta C = \Delta C$ , mass transfer coefficients are readily obtained from present LES data (note that with these definitions we also have  $K_L/u = c/\Delta C$ ). These coefficients are plotted in log–log coordinates in figure 14. This plot clearly shows that  $K_L/u$  is proportional to  $Sc^{-1/2}$  over the whole range of Schmidt numbers explored here.

This result is obviously not new since it may be considered as the major prediction of renewal theories (Highbie 1935; Danckwerts 1951). Nevertheless, as available DNS involving shear-free surfaces mostly considered Schmidt numbers ranging only from 1 to 5, it seems that present results provide one of the first computational evidences supporting this prediction over a wide range of Schmidt number. The  $Sc^{-1/2}$  dependence predicted in the present investigation is also of interest with respect to the LES methodology, as it indicates that the dynamic subgrid-scale model employed here is capable of predicting reliable variations of the mass transfer coefficient irrespective of the Schmidt number, i.e. of the size of the smallest scalar structures. This statement must however be tempered by the fact that the grid we use in the vicinity of the surface is fine enough to capture the small vertical scales of the scalar field (i.e. the simulation is in some sense ‘direct’ in this direction), so that in this crucial region the subgrid-scale model essentially provides the contribution of the unresolved horizontal scales.

Another quantity of interest is the r.m.s. mass transfer fluctuation defined as

$$k_L/u_0 = \frac{D}{u_0 \delta C} \left\langle \left( \frac{\partial c'}{\partial y} \right)^2 \right\rangle^{1/2} \Big|_{y=0}. \quad (7b)$$

This quantity which can hardly be determined in experiments may easily be extracted from the present results by remarking that, owing to the linear growth of the concentration fluctuation in the limit  $Sc^{1/2}y^+ \rightarrow 0$ , the scalar dissipation  $\varepsilon_c$  reduces to  $D\langle(\partial c'/\partial y)^2\rangle$  at the surface. It then turns out that the relative r.m.s. fluctuation of the mass transfer velocity is  $k_L/K_L = (\varepsilon_c^+/2)^{1/2}|_{y=0}$ , with  $\varepsilon_c^+ = D\varepsilon_c/(uc)^2$ . According to figure 6, and disregarding small variations with the Schmidt number caused by subgrid-scale contributions, we conclude that  $k_L/K_L$  is about 0.70, irrespective of the value of  $Sc$ . This indicates that the mass transfer rate at a free surface is a strongly fluctuating quantity, as the magnitude of its fluctuations is of the same order as its average value. Note for the sake of comparison that Calmet & Magnaudet (1997) found the value of  $k_L/K_L$  at a solid wall to decrease consistently from about 0.5 for  $Sc = 1$  to about 0.35 for  $Sc = 200$ .

Coming back to  $K_L$ , we find that the results displayed in figure 14 may be accurately fitted by the simple law

$$K_L/u \approx 0.072Sc^{-1/2}. \quad (8)$$

The prefactor 0.072 was already encountered in the discussion of figure 1 where we observed that the mean velocity profile evolves as  $(1 - \langle \bar{C} \rangle)/\Delta C \approx 0.072y^+Sc^{1/2}$  within the diffusive sublayer. Since we also know from (1) that  $(1 - \langle \bar{C} \rangle)/c = Scy^+$  there, we have  $c/\Delta C = 0.072Sc^{-1/2}$ , in agreement with (8).

To check the accuracy of the prefactor in (8), we critically examined available experimental data sets. In many of them, the mass transfer rate is affected in a subtle way by the presence of surfactants, resulting in values lower than expected at a shear-free interface (even seeding particles used in PIV measurements may contaminate significantly the surface as shown by McKenna & McGillis 2004). Moreover, most of the data obtained in open-channel flows correspond to situations where the bursts emanating from the bottom boundary layer interact directly with the near-surface region and produce ripples on the surface, surprisingly resulting in a lower mass transfer rate as compared with that found with a flat free surface (Knowlton, Gupta & Banerjee 1999). In contrast, as discussed in §1, the situation computed here is similar to that obtained in a grid-stirred tank, so that the most meaningful comparison seems to be with data obtained in such devices. To date, the

best of these data are probably those reported by McKenna & McGillis (2004) who performed extensive simultaneous measurements of the near-surface flow structure (using PIV) and oxygen absorption ( $Sc \approx 490$ ). They also paid particular attention to surface contamination and considered both clean and ‘dirty’ interfaces in the range  $280 \leq Re \leq 10^3$ , approximately. Averaging the various values of  $K_L$  that they obtained with clean interfaces yields, for instance,  $Sc^{1/2}K_L/u = 0.077$  ( $Re = 282$ ) and  $0.066$  ( $Re = 469$ ). Assuming that  $Sc^{1/2}K_L/u$  varies as  $aRe^b$  in between these two Reynolds numbers, we then obtain  $Sc^{1/2}K_L/u \approx 7.15 \times 10^{-2}$  for  $Re = 360$ . This experimental value is in excellent agreement with that corresponding to the LES prediction (8), which provides an additional indication that the important features of the mass transfer process are correctly captured by the present numerical approach.

### 5.2. Relevance of the concept of surface divergence

Obviously, the prefactor in the right-hand side of (8) depends on  $Re$ , and this dependence cannot be directly extracted from our numerical results, since we did not vary the Reynolds number. However the corresponding information can be inferred indirectly by revisiting the analysis of the one-dimensional concentration equation performed by McCreedy *et al.* (1986) in the light of our LES results. Clearly, within the Kolmogorov sublayer, the driving term of this equation may be written as  $\beta(t)y d\langle C \rangle / dy$ ,  $\beta(t)$  denoting the strain rate  $\partial v' / \partial y$ . The question is then to determine which among the other terms in the concentration equation balances the above driving term. In Fourier space, the magnitude of  $\partial c' / \partial t$  at a given frequency  $\omega$  is  $\omega \hat{c}(\omega)$ ,  $\hat{c}(\omega)$  being the corresponding Fourier component of the concentration fluctuation, whereas the magnitude of the diffusive term is  $D \partial^2 \hat{c} / \partial y^2$ . In §3.2, we found that the thickness of the diffusive sublayer throughout which the mean concentration profile is linear is nothing but the Batchelor microscale  $\delta_B = LRe^{-3/4}Sc^{-1/2}$ . As this sublayer is that which determines the mass transfer rate (see (7a)), we can write, for  $y < \delta_B$ ,  $D \partial^2 \hat{c} / \partial y^2 \sim D \hat{c} / \delta_B^2 = \nu Re^{3/2} L^{-2} \hat{c}$ . Using the estimate  $\varepsilon \sim u^3 / L$ , the latter expression may be re-written in the form  $(\varepsilon / \nu)^{1/2} \hat{c}$ , which shows that the characteristic frequency of the vertical diffusion is the Kolmogorov frequency  $f_k = (\varepsilon / \nu)^{1/2}$ . As horizontal diffusion within the diffusive sublayer is driven by large-scale motions, the characteristic frequency of horizontal diffusion is smaller than  $f_k$  by a factor of  $O(Re^{-3/2}Sc^{-1})$ . Similarly, the results of §4, allow us to conclude that the characteristic frequency of the advective terms is  $u/L$ . We thus conclude that in the limit  $y \rightarrow 0$ , vertical diffusion is the dominant term in the concentration equation throughout the whole range of frequencies encountered in the velocity field, i.e. up to the Kolmogorov frequency. Then, defining the Fourier component  $\hat{\beta}(\omega)$  of the vertical velocity gradient and noting that  $d\langle C \rangle / dy \sim \Delta C / \delta_B$ , we have within the Batchelor sublayer,  $\hat{c}(\omega) \sim \delta_B \hat{\beta}(\omega) y \Delta C / D$ . This estimate implies that the co-spectrum  $E_{vc}(\omega)$  of the concentration and vertical velocity fluctuations evolves as  $E_{vc}(\omega) \sim \delta_B E_\beta(\omega) y^2 \Delta C / D$ ,  $E_\beta(\omega)$  denoting the frequency spectrum of  $\beta$ . By virtue of the definition of the inner diffusive sublayer, the turbulent mass flux  $\langle v'c' \rangle = \int_0^\infty E_{vc}(\omega) d\omega$  and the molecular mass flux  $D d\langle C \rangle / dy$  reach equal magnitudes at the outer edge  $y = \delta_B$  of this sublayer, which yields

$$\delta_B \sim D^{1/2} \langle \beta^2 \rangle^{-1/4} \quad (9a)$$

and therefore

$$K_L \sim D^{1/2} \langle \beta^2 \rangle^{1/4}. \quad (9b)$$

The scaling (9b) was first obtained by McCready *et al.* (1986) who suggested that it is valid for the part of the concentration spectrum corresponding to ‘low enough’ frequencies. What our LES results indicate is that (9b) is actually valid throughout the whole spectrum, since the diffusion term exceeds the time-rate-of-change term up to the Kolmogorov frequency  $f_k$ . Hence the ‘renewal’ frequency  $\tau^{-1}$  involved in the Highbie–Dankwerts model is confirmed to be  $\langle\beta^2\rangle^{1/2}$ . A convincing experimental support to this conclusion was provided by McKenna & McGillis (2004) under a broad range of hydrodynamic conditions (flat or wavy surface, with or without surfactants).

Note that if the thickness of  $\delta_B$  were varying as  $LR e^{-1/2} Sc^{-1/2}$  (i.e. the mass transfer rate were governed by the outer diffusive layer rather than the Batchelor sublayer), the above analysis would imply that the time-rate-of-change term would dominate over the diffusive term for  $\omega > u/L$ . This would result in a mass transfer velocity

$$K_L \sim D^{1/2} \left( \int_0^\infty (E_\beta(\omega)/\omega) d\omega \right)^{1/2} \sim D^{1/2} (E_\beta(0))^{1/2}$$

instead of (9b), meaning that only the low-frequency contribution to the surface divergence would contribute to  $K_L$ . This makes it clear that the crucial reason why the mass transfer rate depends on the cumulative strain rate  $\langle\beta^2\rangle$  and not only on its low-frequency (or low-wavenumber) contents is because the inner diffusive sublayer scales as  $Re^{-3/4}$ .

To compare our results with the theoretical model (9b), we need the r.m.s. value of the surface divergence. This information is provided by figure 3 of CM which indicates (after a proper renormalization in terms of  $u$  instead of  $u^*$ )  $(\langle v^2 \rangle^{1/2}/y)_{y=0} = \langle\beta^2\rangle^{1/2} \approx .015u^2/\nu$ . Using this result, we may re-write (8) in the form

$$K_L/u \approx 0.6Sc^{-1/2} (\nu\langle\beta^2\rangle^{1/2}/u^2)^{1/2}. \quad (10)$$

The prefactor  $\alpha = 0.6$  is in good agreement with that obtained by McCready *et al.* ( $\alpha = 0.7$ ) who solved numerically the concentration equation forced by an experimental velocity signal. The slight difference between the two values may have a number of causes, since McCready *et al.* made several important simplifying assumptions (two-dimensional flow,  $E_\beta(\omega)$  taken from a near-wall signal, spanwise variation of the velocity fluctuations represented by a single harmonic with a wavelength equal to that of near-wall streaks, . . .). On the other hand, our LES procedure may slightly underestimate the mass transfer rate since the horizontal small-scale motions are not directly computed, and this may result in a somewhat lower value of  $\alpha$ .

Let us finally examine the consequences of (10) in terms of the dependence of the mass transfer rate with respect to the Reynolds number. Comparing (9a) with the definition of the Batchelor microscale  $\delta_B = LR e^{-3/4} Sc^{-1/2}$  and making use of the estimate  $\varepsilon \sim u^3/L$  yields immediately  $\langle\beta^2\rangle \sim \varepsilon/\nu$ . This allows us to re-express (10) in the form

$$K_L/u = \alpha Sc^{-1/2} Re^{-1/4}, \quad (11)$$

where  $\alpha$  is an  $O(1)$  constant. According to our LES results, the value of  $\alpha$  required to recover (10) quantitatively is 0.31, which is close to the ‘optimal’ value  $\alpha = 0.25$  suggested by Theofanous *et al.* (1976). Equation (11) makes it clear that the surface divergence model (10) of McCready *et al.* (1986) predicts the same dependence of the mass transfer rate *vs.* the turbulent Reynolds number as the ‘small-scale eddy’ model of Banerjee *et al.* (1968) and Lamont & Scott (1970). However, this point must not be misunderstood. In §4, we showed that the structures that drive the

near-surface concentration field are the large-scale updraughts and downdraughts. In this sense it is clear that the mass transfer rate is controlled by the large-scale events, as shown experimentally by Komori *et al.* (1989). However, the vertical movements of these structures strongly mix the upper layers of the flow and what we observed in §3.2 is that the efficiency of this mixing process reduces the thickness of the diffusive sublayer to about one Batchelor microscale. This is the reason why the exponent  $-1/4$  occurs in (11) and it must be kept in mind that this exponent does not imply that the transfer is controlled by the small-scale eddies. Note that the  $Re$ -dependence indicated by (11) is weak, so that it may be altered by a number of factors, among which are the turbulence anisotropy below the surface-influenced region and the deformation of the free surface. This is why the best support to the above  $Re$ -exponent is generally provided by grid-stirred experiments where the above alterations are small. For instance, the aforementioned experiments of McKenna & McGillis (2004) corresponding to a clean interface display an average  $Re$ -exponent of  $-0.26$  in the range  $280 < Re < 900$ . In contrast, turbulence anisotropy and surface deformation (in low-depth experiments) prevent most of the open-channel data from displaying a clear variation of  $K_L/u$  vs.  $Re$ . For instance, the results of Komori *et al.* (1989) are found to be almost  $Re$ -independent when plotted in dimensionless form. Similarly, a direct comparison between the mass transfer rate predicted by the DNS of Handler *et al.* (1999) ( $Re=95$ ,  $Sc=2$ ) and (8) yields a  $Re$ -exponent of about  $-0.13$ , i.e. half that predicted by (11). However, in this DNS the r.m.s. vertical velocity at  $y=L$  (say  $v$ ) is such that  $v/u \approx 0.75$  whereas  $v/u \approx 0.9$  in our LES. If we crudely assume that  $\langle \beta^2 \rangle (L/u)^2$  is proportional to  $(v/u)^2$  (an assumption consistent with the Hunt–Graham (1978) theory discussed below), the  $Re$ -exponent becomes  $-0.20$ , which is much closer to the prediction in (11). A detailed investigation of the influence of the turbulence anisotropy on the relationship between the mass transfer rate and the turbulent Reynolds number is beyond the scope of the present work, but the above estimate clearly suggests that this parameter has a strong influence and must be taken into account for generalizing (11) to flows where the turbulence is significantly anisotropic. Finally, it is worth noting that (11) (through the estimate  $\langle \beta^2 \rangle \sim \varepsilon/\nu$ ), relies on the assumption of a well-developed inertial subrange in the turbulence spectrum  $E(k)$ . If  $Re$  is too low for such a subrange to exist,  $E(k)$  exhibits a larger negative slope and straightforward calculations of  $\langle \beta^2 \rangle$  assuming  $E(k) \propto k^{-m}$  with  $m > 5/3$  indicate that the larger  $m$ , the larger the negative exponent of the Reynolds number in (11). This confirms the conclusion of Theofanous *et al.* (1976) that the  $Re^{-1/4}$  scaling is characteristic of high Reynolds numbers, whereas mass transfer rates determined in low- $Re$  experiments exhibit a larger variation with the Reynolds number.

### 5.3. The connection between the r.m.s. surface divergence and the underlying turbulence

The last question to which our computations may contribute is that of the relationship between the value of the r.m.s. surface divergence and the bulk turbulence. This question may be summarized in the form: given the values of the large-scale properties  $u$  and  $L$  of the turbulence below the surface-influenced region (still assuming that this turbulence is isotropic), what is the value of  $\langle \beta^2 \rangle$ ? A general answer to this question is desirable since it would open the possibility of estimating directly the mass transfer rate through (10), without a need to investigate the detailed structure of the Kolmogorov sublayer. Some attempts to address this question have already been made (Brumley & Jirka 1988; Banerjee 1990; Banerjee *et al.* 2004), but we think a

re-examination in the light of recent theoretical analyses and of present LES results may clarify the problem.

As we saw above,  $\langle \beta^2 \rangle$  scales as  $\varepsilon/\nu$  for high enough  $Re$ . This is consistent with the usual estimate of the variance of velocity gradients in homogeneous isotropic turbulence, where  $\langle (\partial v'/\partial y)^2 \rangle = 1/15(\varepsilon/\nu)$  (Batchelor 1953, p. 47). However, the prefactor 1/15 cannot subsist in the near-surface region, since the turbulence structure is modified by two different phenomena. The first of these, whose effects extend approximately over one integral scale below the surface, is the blocking process that forces the vertical velocity to vanish at the surface. The consequences of this purely kinematic process on the statistical structure of the turbulence were described by Hunt & Graham (1978). They were revisited by Magnaudet (2003) who examined in particular the variance of velocity gradients throughout the so-called ‘source layer’ extending approximately from  $y=L$  to the edge of the viscous sublayer  $y=2.0Re^{-1/2}L$ . His analysis shows that even though the r.m.s. vertical velocity fluctuation falls from its free-stream value at  $y=L$  to tiny values at  $y=2.0Re^{-1/2}L$ , the r.m.s. of the vertical gradient  $\partial v'/\partial y$  does not change significantly because only eddies larger than the Taylor microscale are blocked by the surface in this region. In contrast, within the Kolmogorov sublayer, the blocking effect affects all wavenumbers and tends to greatly increase  $\partial v'/\partial y$ . The variance of the velocity gradients at the surface can easily be evaluated from the Hunt–Graham theory. In particular, we find  $\langle (\partial v'/\partial y)^2 \rangle|_{y=0} = 1/3(\varepsilon/\nu)$ , a result suggesting that  $\langle (\partial v'/\partial y)^2 \rangle$  increases by a factor of five from  $y=2.0Re^{-1/2}L$  to  $y=0$  (Brumley & Jirka 1988) (note that in the above estimate,  $\varepsilon$  denotes the dissipation rate in the bulk). Mass transfer models based on this ‘inviscid’ estimate of the surface divergence have been proposed by Banerjee (1990) and Banerjee *et al.* (2004). However, these models overlook the second near-surface process, namely the viscous damping of the horizontal components of the vorticity within the viscous sublayer. Viscous corrections to the Hunt–Graham model were derived by Teixeira & Belcher (2000) in the time-dependent situation corresponding to the development of a shear-free boundary layer created by the sudden insertion of a surface onto an initially homogeneous isotropic turbulence. These authors showed that viscous effects affect primarily eddies whose size  $k^{-1}$  is comparable to or smaller than the thickness  $\delta_V(t)$  of the viscous sublayer. Unfortunately, the quantitative validity of their corrections is limited to the very early stages of the motion during which  $\delta_V(t)$  is still smaller than the Kolmogorov length scale  $\delta_K$ . Nevertheless their theoretical expressions make it clear that, while the r.m.s. horizontal velocities which are mainly determined by the large scales are only weakly affected by viscous effects (the relative magnitude of the corresponding correction is  $O(Re^{-1/2})$ ), all non-zero velocity gradients experience an  $O(1)$  reduction when  $\delta_V(t) \sim \delta_K$ . More precisely, their figure 6(d) indicates that  $\langle \beta^2 \rangle$  is reduced by a factor of two approximately, compared to the inviscid prediction. There appears to be no reason to suspect that the nonlinear effects which are negligible during this very early stage of the flow may remove or even reduce this viscous effect, since the nonlinear processes usually mostly stop the growth of the flow characteristics at the value they had at the end of the linear stage. Moreover, the same reduction by a factor of two is observed at later stages of the flow in the DNS of Perot & Moin (1995) and Walker, Leighton & Garza-Rios (1996).

To detect the consequences of the processes discussed above in our LES results, we first require the value of the dissipation rate  $\varepsilon$  in the source layer (as shown by Magnaudet (2003), this value is almost identical to the bulk value). Figure 5(a) of CM indicates  $\varepsilon \approx 1.87 \times 10^{-3}u^4/\nu$ , from which according to the ‘inviscid’ predictions discussed above,  $\langle (\partial v'/\partial y)^2 \rangle^{1/2}$  should vary from  $1.1 \times 10^{-2}u^2/\nu$  (corresponding to

the homogeneous isotropic estimate) at the outer edge of the viscous sublayer to  $2.5 \times 10^{-2} u^2/\nu$  at the surface (corresponding to the ‘inviscid’ surface prediction). As we previously found  $\langle \beta^2 \rangle^{1/2} = 1.5 \times 10^{-2} u^2/\nu$ , we see that the value of the r.m.s. surface divergence provided by the LES is well in the range of these theoretical predictions. However, it lies significantly below the ‘inviscid’ surface value, which is not unlikely given the above discussion. According to the numerical value of  $\langle \beta^2 \rangle$ , we infer that viscous effects reduce  $\langle (\partial v'/\partial y)^2 \rangle$  by a factor of 2 to 3, i.e. the actual value of  $\langle \beta^2 \rangle$  lies approximately in the range  $[\varepsilon/9\nu, \varepsilon/6\nu]$ . While this estimate is provisional at the present stage and probably depends somewhat on the Reynolds number, it is qualitatively in line with the results of Teixeira & Belcher (2000). Consequently, our results confirm that the inviscid blocking effect and the viscous near-surface reduction of the velocity gradients have to be considered together if we are seeking reliable quantitative estimates of  $\langle \beta^2 \rangle$  capable of predicting directly the mass transfer rate through (10).

## 6. Summary and concluding remarks

The results discussed in this paper provide a detailed view of the mechanisms governing the mass transfer process through a flat shear-free surface bounding a turbulent flow where the bulk turbulence is approximately isotropic. The numerical data were obtained for a wide range of Schmidt number (1 to 200), and for a single turbulent Reynolds number of 360. These results first established the dependence of several statistical quantities *vs.* the Schmidt number. In line with theoretical arguments, the thickness of the inner diffusive sublayer and the mass transfer rate were found to be proportional to  $Sc^{-1/2}$ . Similarly, when plotted against the dimensionless distance  $Sc^{1/2}yu/\nu$ , the near-surface profiles of the normalized concentration variance and of all terms contributing to its budget were shown to be independent of the Schmidt number. The simultaneous analysis of the near-surface concentration and velocity fluctuations emphasized the role of the large-scale updraughts and downdraughts. In particular, it revealed the one-to-one correspondence between the vertical motions that penetrate the inner diffusive layer and the near-surface concentration fluctuations, each mirroring the other. The co-spectra of  $c''$  and  $v''$  also provided an unambiguous indication that the mass transfer process is driven by motions whose spatial extension in the horizontal directions is about  $2L$ , i.e. large-scale motions. A third series of results concerned the role of the turbulent Reynolds number. Whereas our computations were carried out for a single Reynolds number, comparison of the thickness of the various dynamic and concentration sublayers, combined with available low- $Re$  DNS data, allowed us to establish the  $Re$ -variation of the inner and outer diffusive sublayers. It turned out that the thickness of the inner diffusive sublayer throughout which the mean concentration profile is linear, is about  $2.0Sc^{-1/2}Re^{-3/4}$ , i.e. it corresponds to the Batchelor microscale. In contrast, the thickness of the outer diffusive layer throughout which the r.m.s. fluctuation grows from zero at the surface to a maximum at the outer edge is about  $2.0Sc^{-1/2}Re^{-1/2}$ . By a frequency analysis of the concentration equation, we showed that the  $Re^{-3/4}$  scaling of the inner diffusive sublayer results directly in the  $\langle \beta^2 \rangle^{1/4}$  scaling of the mass transfer velocity  $K_L$ , which in turns implies that  $K_L$  is proportional to  $Re^{-1/4}$ . As pointed out in § 5, while this  $Re^{-1/4}$  scaling is identical to that predicted by the ‘small-eddy’ model, it just results from the  $Re$ -variation of the thickness of the inner diffusive sublayer and implies by no means that the transfer is governed by small-scale eddies (equivalently, we may say that the only ‘small scale’ relevant in the mass transfer process is the thickness of the inner diffusive sublayer).

Finally, our investigation, combined with available DNS and theoretical results, was found to provide some indication of the influence of turbulence anisotropy and near-surface viscous effects on the mass transfer rate.

Obviously, present results have a fairly limited range of direct applicability since they were obtained for a flat shear-free surface, whereas in practice most gas–liquid interfaces are (at least intermittently) subject to shear and deformation, or even to wave breaking. If air is blowing above the surface and induces an interfacial shear stress  $\rho u_i^2$  in the liquid ( $\rho$  being the liquid density), our results are, in principle, valid only if  $u_i/u \ll 1$ . Similarly, if  $u_w$  denotes the interfacial r.m.s. velocity fluctuation induced by the vertical displacements of the surface, the assumption of a flat surface only holds in the limit  $u_w/u \ll 1$ . Situations in which  $u$  exceeds  $u_i$  and  $u_w$  correspond, for instance, to low-wind stages where the main instantaneous source of mixing comes from the turbulence in the upper layer of water rather than from the surface itself, whatever the precise origin of this turbulence. Clearly, a general model of mass transfer must also encompass situations in which the driving mechanism of the transfer is provided by the interfacial shear ( $u_i \gg \text{Max}(u, u_w)$ ) or the waves that propagate at the surface ( $u_w \gg \text{Max}(u, u_i)$ ), as well as more complicated situations in which several of these mechanisms act simultaneously. In the case where  $u_i \gg \text{Max}(u, u_w)$ , the near-surface turbulent field resembles that near a solid wall, including the presence of longitudinal streaks (Lam & Banerjee 1992), except that horizontal fluctuations do not return to zero at the surface. The mass transfer process through a flat sheared interface was investigated numerically by Calmet & Magnaudet (1998) and Lakehal *et al.* (2003). In this situation, the relevant velocity and length scales of the surface boundary layer are  $u_i$  and  $\nu/u_i$ , respectively. Therefore, when scaled properly with the above inner variables, the mass transfer rate does not depend on any outer turbulent Reynolds number, which contrasts with the  $Re^{-1/4}$  dependence typical of the shear-free case. Hence, similarly to the case of a wall-bounded shear flow, the prediction of the mass transfer rate in the limit  $u_i \gg \text{Max}(u, u_w)$  turns out to be simpler than that through a shear-free surface because the turbulence is generated directly in the region of interest.

The question of how surface deformation and surface waves affect the mass transfer process is much more complicated. In particular, the problem is obscured in most experiments by the intrinsic coupling between wave generation and interfacial shear. However, recent experiments in which standing capillary waves were generated by a Faraday instability at the surface of an otherwise quiescent liquid demonstrated unambiguously that such waves may tremendously increase the mass transfer rate (Saylor & Handler 1999). What remains unclear is the mechanism responsible for this enhancement. Among others, plausible candidates are random surface drift due to wave modulation (e.g. Ramshankar & Gollub 1991), flow separation induced by vorticity generation on a strongly curved free surface (Longuet-Higgins 1992), or advection-enhanced diffusion due to the alternatively converging/diverging streamlines below the waves (Szeri 1997). Future computational studies may substantially help to explore the impact of the above mechanisms. For instance, using the curvilinear version of our code (e.g. Merle, Legendre & Magnaudet 2005), the present LES approach can be extended to the case where the surface is populated with periodic capillary waves with arbitrary amplitude and frequency. The advantage of such an approach is that the ratio  $u_w/u$  and the wave characteristics can be varied arbitrarily, making it possible to disentangle the respective role of several possible mechanisms and to explore a significant range of parameters in order to derive scaling laws for the mass transfer rate. We believe that such approaches

combined with laboratory experiments may significantly contribute to improving the understanding and the prediction of mass transfer in real geophysical and industrial systems.

## REFERENCES

- ASHER, W. E. & PANKOW, J. F. 1986 The interaction of mechanically generated turbulence and interfacial films with a liquid phase controlled gas/liquid transport process. *Tellus* **38B**, 305–318.
- ATMANE, M. & GEORGE, J. 2002 Gas transfer across a zero-shear surface: a local approach. In *Gas Transfer at Water Surfaces* (ed. M. A. Donelan *et al.*), pp. 255–259. Geophysical Monographs Series.
- BANERJEE, S. 1990 Turbulence structure and transport mechanisms at interfaces. *Proc. Intl Conf. Heat Transfer, Jerusalem* (ed. G. Hetsroni), pp. 395–418.
- BANERJEE, S., LAKEHAL, D. & FULGOSI, M. 2004 Surface divergence models for scalar exchange between turbulent streams. *Intl J. Multiphase Flow* **30**, 963–977.
- BANERJEE, S., RHODES, R. & SCOTT, D. S. 1968 Mass transfer to falling wavy liquid films in turbulent flows. *Ind. Engng Chem. Fund.* **7**, 22–26.
- BATCHELOR, G. K. 1953 *The Theory of Homogeneous Turbulence*. Cambridge University Press.
- BORUE, V., ORSZAG, S. A. & STAROSELSKY, I. 1995 Interaction of surface waves with turbulence: direct numerical simulations of turbulent open-channel flow. *J. Fluid Mech.* **286**, 1–23.
- BRUMLEY, B. H. & JIRKA, G. H. 1987 Near surface turbulence in grid-stirred tank. *J. Fluid Mech.* **183**, 235–263.
- BRUMLEY, B. H. & JIRKA, G. H. 1988 Air–water transfer of slightly soluble gases: turbulence, interfacial processes and conceptual models. *PhysicoChem. Hydrodyn.* **10**, 295–319.
- CALMET, I. & MAGNAUDET, J. 1997 Large-eddy simulation of high-Schmidt number mass transfer in a turbulent channel flow. *Phys. Fluids* **9**, 438–455.
- CALMET, I. & MAGNAUDET, J. 1998 High-Schmidt number mass transfer through turbulent gas-liquid interfaces. *Intl J. Heat Fluid Flow* **19**, 522–532.
- CALMET, I. & MAGNAUDET, J. 2003 Statistical structure of high-Reynolds-number turbulence close to the free surface of an open-channel flow. *J. Fluid Mech.* **474**, 355–378 (referred to herein as CM).
- CAMPBELL, J. A. & HANRATTY, T. J. 1983 Mechanism of turbulent mass transfer at a solid boundary. *AIChE J.* **29**, 221–223.
- CHU, C. R. & JIRKA, G. H. 1992 Turbulent gas flux measurements below the air-water interface of a grid-stirred tank. *Intl J. Heat Mass Transfer* **35**, 1957–1968.
- COANTIC, M. 1986 A model of gas transfer across air–water interfaces with capillary waves. *J. Geophys. Res.* **91**, 3925–3943.
- DANCKWERTS, P. V. 1951 Significance of liquid film coefficients in gas absorption. *Ind. Engng Chem.* **43**, 1460–1466.
- DAVIES, J. T. 1972 *Turbulence Phenomena*. Academic.
- FORTESCUE, G. E. & PEARSON, J. R. A. 1967 On gas absorption into a turbulent liquid. *Chem. Engng Science* **22**, 1163–1176.
- GERMANO, M. 1986 A proposal for a redefinition of the turbulent stresses in the filtered Navier–Stokes equations. *Phys. Fluids* **29**, 2323–2324.
- GERMANO, M. 1992 Turbulence: the filtering approach. *J. Fluid Mech.* **238**, 325–336.
- HANDLER, R. A., SAYLOR, J. R., LEIGHTON, R. I. & ROVELSTAD, A. L. 1999 Transport of a passive scalar at a shear-free boundary in fully turbulent open channel flow. *Phys. Fluids* **11**, 2607–2625.
- HANDLER, R. A., SWEAN, T. F., LEIGHTON, R. I. & SWEARINGEN, J. D. 1993 Length scales and the energy balance for turbulence near a free surface. *AIAA J.* **31**, 1998–2007.
- HERLINA & JIRKA, G. H. 2004 Application of LIF to investigate gas transfer near the air–water interface in a grid-stirred tank. *Exps. Fluids* **37**, 341–349.
- HIGHBIE, R. 1935 The rate of absorption of a pure gas into a still liquid during short periods of exposure. *Trans. AIChE* **31**, 365–388.

- HUNT, J. C. R. 1984 Turbulence structure and turbulent diffusion near gas-liquid interfaces. In *Gas Transfer at Water Surfaces* (ed. W. Brutsaert & G. H. Jirka), pp. 67–82. Reidel.
- HUNT, J. C. R. & GRAHAM, J. M. R. 1978 Free stream turbulence near plane boundaries. *J. Fluid Mech.* **84**, 209–235.
- KNOWLTON, B., GUPTA, R. & BANERJEE, S. 1999 Estimation of the free surface mass transfer coefficients using experimental DPIV velocity data. In *Proc. Turb. and Shear Flow Phenomena 1*, (ed. S. Banerjee & J. K. Eaton), pp. 461–465. Begell House.
- KOMORI, S., MURAKAMI, Y. & UEDA, H. 1989 The relationship between surface-renewal and bursting motions in an open-channel flow. *J. Fluid Mech.* **203**, 103–123.
- KOMORI, S., NAGAOSA, R., MURAKAMI, Y., CHIBA, S., ISHII, K. & KUWAHARA, K. 1993 Direct numerical simulation of three-dimensional open-channel flow with zero-shear gas-liquid interface. *Phys. Fluids A* **5**, 115–125.
- KUMAR, S., GUPTA, R. & BANERJEE, S. 1998 An experimental investigation of the characteristics of free-surface turbulence in channel flow. *Phys. Fluids* **10**, 437–456.
- LAKEHAL, D., FULGOSI, M., YADIGAROGU, G. & BANERJEE, S. 2003 Direct numerical simulation of turbulent heat transfer across a mobile, sheared gas-liquid interface. *J. Heat Transfer* **125**, 1129–1139.
- LAM, K. & BANERJEE, S. 1992 On the conditions of streak formation in a bounded turbulent flow. *Phys. Fluids A* **4**, 306–320.
- LAMONT, J. C. & SCOTT, D. S. 1970 An eddy cell model of mass transfer into the surface of a turbulent liquid. *AIChE J.* **16**, 513–519.
- LEVICH, V. G. 1962 *Physicochemical Hydrodynamics*. Prentice-Hall.
- LONGUET-HIGGINS, M. S. 1992 Capillary rollers and bores, *J. Fluid Mech.* **240**, 659–679.
- LU, D. M. & HETSRONI, G. 1995 Direct numerical simulation of a turbulent open channel flow with passive heat transfer. *Intl J. Heat Mass Transfer* **38**, 3241–3251.
- MCCREADY, M. J., VASSILIADOU, E. & HANRATTY, T. J. 1986 Computer simulation of turbulent mass transfer at a mobile interface. *AIChE J.* **32**, 1108–1115.
- MCKENNA, S. P. & MCGILLIS, W. R. 2004 The role of free-surface turbulence and surfactants in air–water gas transfer. *Intl J. Heat Mass Transfer* **47**, 539–553.
- MAGNAUDET, J. 2003 High-Reynolds-number turbulence in a shear-free boundary layer: revisiting the Hunt–Graham theory. *J. Fluid Mech.* **484**, 167–196.
- MERLE, A., LEGENDRE, D. & MAGNAUDET, J. 2005 Forces on a high-Reynolds-number spherical bubble in a turbulent flow. *J. Fluid Mech.* **532**, 53–62.
- MONIN, A. S. & YAGLOM, A. M. 1975 *Statistical Fluid Mechanics*. MIT Press.
- NAGAOSA, R. 1999 Direct numerical simulation of vortex structures and turbulent scalar transfer across a free surface in a fully developed turbulence. *Phys. Fluids* **11**, 1581–1595.
- PAN, Y. & BANERJEE, S. 1995 A numerical study of free surface turbulence in channel flow. *Phys. Fluids* **7**, 1649–1664.
- PEROT, B. & MOIN, P. 1995 Shear-free turbulent boundary layers. Part I. Physical insights into near-wall turbulence. *J. Fluid Mech.* **295**, 199–227.
- RAMSHANKAR, R. & GOLLUB, J. P. 1991 Transport by capillary waves. Part II. Scalar dispersion and the structure of the concentration field. *Phys. Fluids A* **3**, 1344–1350.
- SAYLOR, J. R. & HANDLER R. A. 1999 Gas transport across an air/water interface populated by capillary waves. *Phys. Fluids* **9**, 2529–2541.
- SMAGORINSKI, 1963 General circulation experiments with the primitive equations. *Mon. Weather Rev.* **91**, 99–164.
- SZERI, A. 1997 Capillary waves and air–sea gas transfer. *J. Fluid Mech.* **332**, 341–358.
- TEIXEIRA, M. A. C. & BELCHER, S. E. 2000 Dissipation of shear-free turbulence near boundaries. *J. Fluid Mech.* **422**, 167–191.
- TENNEKES, N. H. & LUMLEY, J. L. 1972 *A First Course in Turbulence*. MIT Press.
- THEOFANOUS, T. G., HOUIZE, R. N. & BRUMFIELD, L. K. 1976 Turbulent mass transfer at free, gas-liquid interfaces, with applications to open-channel, bubble and jet flows. *Intl J. Heat Mass Transfer* **19**, 613–624.
- WALKER, D. T., LEIGHTON, R. I. & GARZA-RIOS, L. O. 1996 Shear-free turbulence near a flat free surface. *J. Fluid Mech.* **320**, 19–51.

- WOODROW, P. T. & DUKE, S. R. 2001 Laser-induced fluorescence studies of oxygen transfer across unsheared flat and wavy air–water interfaces. *Ind. Engng Chem. Res.* **40**, 1985–1995.
- YAGLOM, A. M. & KADER, B. A. 1974 Heat and mass transfer between a rough wall and turbulent fluid flow at high Reynolds and Péclet numbers. *J. Fluid Mech.* **62**, 601–623.
- YAMAMOTO, Y., KUNUGI, T. & SERIZAWA, A. 2001 Turbulence statistics and scalar transport in an open-channel flow. *J. Turbulence* **2**, 010.
- ZANG, Y., STREET, R. L. & KOSEFF, J. R. 1993 A dynamic mixed subgrid-scale model and its application to turbulent recirculating flows. *Phys. Fluids A* **5**, 3186–3196.